5 Intercalation

The principal mechanisms involved in the intercalation reaction have been summarized in Chap. 2. In this chapter the results obtained with intercalation experiments will be reported, while the influence on the electronic structure will be discussed in more detail in Chapter 6. To have a reference, model experiments based on alkali deposition on single crystals have been performed first. Different layered dichalcogenides and different alkali metals were studied. Details on the intercalation mechanisms and the driving force of intercalation were also provided by co-deposition experiments. The advantages of using thin films as a substrate will be shown in the following section. Finally *in-situ* electrochemical intercalation will be reported, which was achieved for the first time in this work.

5.1 Deposition on single crystals

Na deposition on single crystals was performed on the sulfides and selenides of Ti and Ta, as representative of group IVb and Vb TMDCs. All investigated compounds are metallic, which is important, since guest insertion is favored by a high electronic conductivity.

Given the now abundant literature on PES investigations of UHV-intercalated TMDCs, some data on the investigated systems was already available. Results of relevance to this work will be briefly reviewed to introduce each system.

5.1.1 Na/TiS_2

Weitering and Hibma investigated Na deposition onto TiS_2 (0001) single crystal surfaces first [90]. Na was found to form an ordered ($\sqrt{13} \times \sqrt{13}$) superstructure if the substrate was kept at –145°C, but was readily intercalated at room temperature. They observed an increase of the DOS at E_F, a broadening of the Ti 2p core level, and a shift of the S 2p core level to higher BE. The system Na/TiS_2 has also recently been investigated with angle-resolved SXPS by Brauer *et al.* [47]. In disagreement to the previous work a shift of the S 2p level to lower BE and of Ti 3p to higher BE is reported. The authors do not discuss this inconsistency, and it is doubtful whether the higher surface sensitivity they used (due to the lower photon energy) can explain it. Both measurements were performed with single crystals and for maximal intercalation. A comparison of the experimentally obtained electronic structures by angle-resolved photoemission with calculations for the fully-intercalated $NaTiS_2$ was also attempted, and fair agreement was found, indicating that the rigid band model may still be used qualitatively. However, while calculations for $NaTiS_2$ indicated some residual dispersion perpendicular to the layers, experimentally no dispersion was found at all.

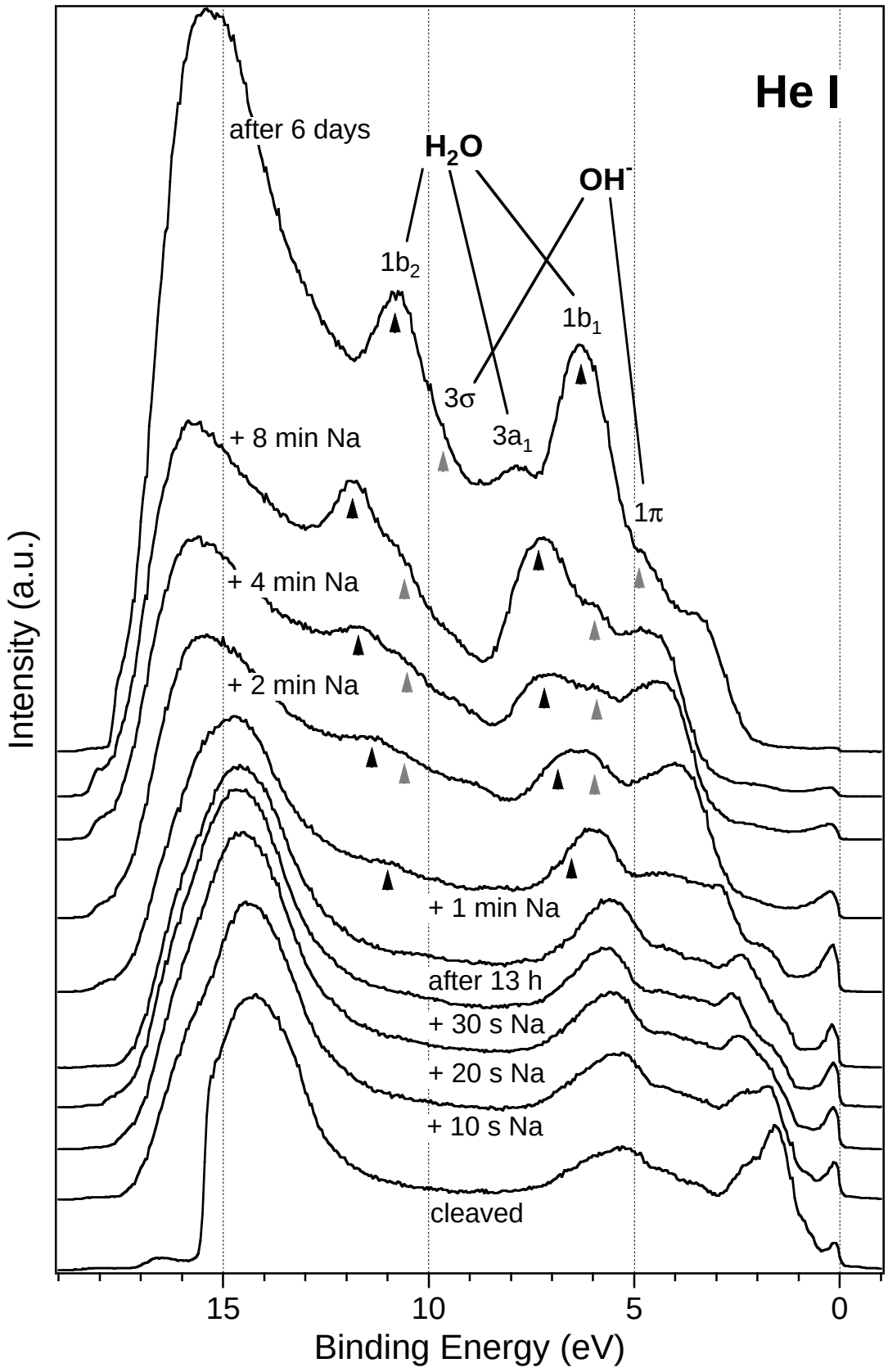

Fig. 5.1 Valence band spectra measured with an excitation energy of 21.2 eV (He I) on a cleaved TiS_2 crystal after stepwise deposition of increasing amounts of Na or after resting times. Marks identify the most intense molecular emission lines of H_2O (black) and of OH^- (gray)

TiS_2 crystals used for the experiments here reported were nearly 1 cm large, they were thick and rigid, and large mirror-like surfaces were obtained by cleavage. Possibly a consequence of self-intercalation was that TiS_2 cleavage required an unusual strength, compared to the other studied single crystals. As alkali metals, also excess Ti is expected to strengthen the intra-layer cohesion due to its electrostatic interaction with the host lattice. Valence band spectra in dependence of Na deposition are reported in Fig. 5.1. The intense peak in the spectrum for the cleaved pristine crystal just below E_F gives evidence of large self-intercalation. Based on the empirical equation given in ref. [158] for $Ti_{1+x}S_2$

$$E_{CB} - E_F = -0.67 - 0.24 \cdot \ln(x + 0.02) \qquad \textit{(Eq. 5.1)},$$

an onset of the Ti 3d band at 0.3 eV below E_F corresponds to $Ti_{1.2}S_2$. This is consistent with the results of RBS measurements on crystals prepared in other batches with the same method.

For the early stage of the experiment (up to Na doses of 30 s and the first rest time of 13 h) the spectral changes show the expected behavior of intercalation; the details will be discussed below. For longer deposition times the valence spectra are covered by intense new peaks that can be assigned to O 2p states related to H_2O adsorption from the residual gas in the vacuum [209]. In fact, O 1s spectra reported in Fig. 5.2 also show two components, marked in analogy with Fig. 5.1. The intensities of the H_2O and OH^- components have a similar development in both sets of spectra. Depending on the substrate and the experimental conditions water can interact with a solid surface in different ways, including dissociative adsorption and the formation of ice layers with intermolecular H-bonding [209]. In presence of traces of Na water typically adsorbs without dissociation, while for larger amounts a decomposition to OH^- and H_2 occurs [210, 211]. Due to the transfer of Na 3s electrons to the substrate, small Na amounts forming Na^+ adatoms do not dissociate H_2O. But with larger amounts of deposited Na the reducing power is high enough for a reaction with H_2O. Once NaOH is formed further water adsorbs to it. NaOH is known to have high solvation enthalpy, and in wet atmosphere several molecules may attach to a single NaOH unit. Thus, in our case with increasing Na doses an increasing Na amount must be present at the surface, and eventually NaOH interacting with H_2O forms. In the He I spectra two couple of peaks can be identified to develop. According to refs. [209, 210] the couple at higher BE are the $1b_2$ and $1b_1$ molecular states of water, while the low BE couple are 3σ and 1π states of OH^-. After long residence in the chamber water continues to adsorb, and the whole valence band structure resembles that of adsorbed ice layers; in this case also the weaker $3a_1$ state can be clearly identified. The emission lines of the O 1s spectra can be assigned in agreement to the valence band spectra. In the last spectra the OH^- emission compared to H_2O is apparently more intense in O 1s than in He I. The

O 1s emission line is less surface sensitive, and may include a further component related to the substrate hydrolysis to TiO_2 (see below).

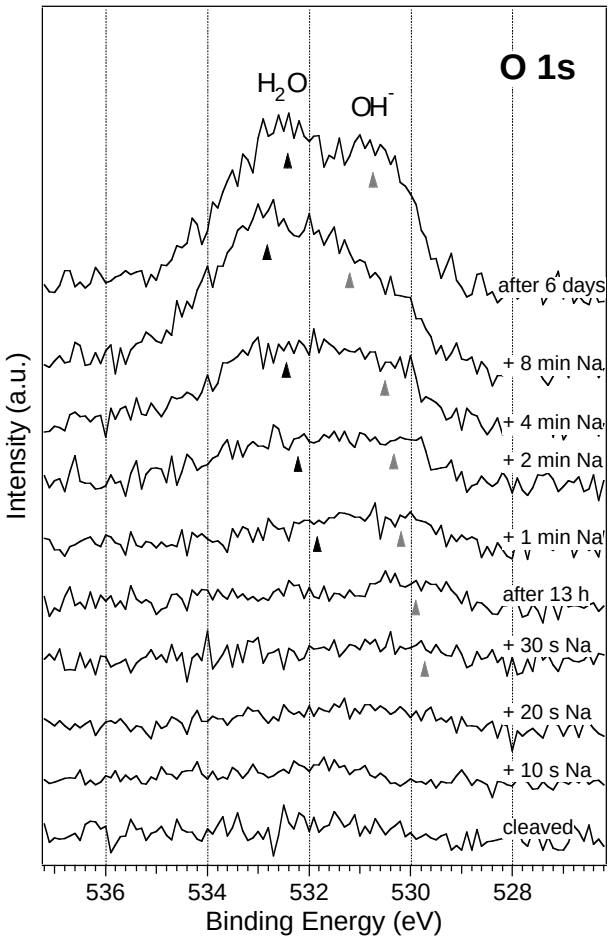

Fig. 5.2 O 1s XPS spectra of a cleaved TiS_2 crystal after stepwise deposition of increasing amounts of Na or after resting times. Marks identify the most intense molecular emission lines of H_2O (black) and of OH^- (gray)

The decrease of the emission intensity at the Fermi level for longer deposition times indicates that the coverage by $NaOH/H_2O$ extends to a larger fraction of the sample surface. Any evaluation of the substrate valence structure with intercalation can be done only for the early deposition steps. In order to better evaluate the spectral modifications, He I spectra for low H_2O coverage (corresponding to Na/Ti concentrations below 0.4, see below) have been reported in Fig. 5.3. In this figure the spectra are represented with the same intensity axis, and are only shifted in their energy axis, until an overlap of the Ti 3d band (marked as 'A') was obtained. With this shift it is clearly evident how the shape of band A does not change remarkably, and its intensity increases just due to the filling of originally empty conduction band states by electrons transferred from the intercalated Na. The E_F shift observed within this intercalated Na amount is of 0.35 eV. A similar shift was found with XANES measurements in the fully intercalated $LiTiS_2$ by Moreau *et al.* [81]. The valence region marked by peaks B-D corresponds to the bands originated by the 12 valence electrons of the stoichiometric TiS_2 compound. According to several theoretical calculations [40, 41, 43, 44, 46] they have mainly the character of S 3p states with a weak Ti 3d admixture. These

band structure calculations indicate that S orbitals overlap relatively strong along the **c** axis, and this leads to a large energy dispersion of the related bands in the **k**-space (see Chap. 2). In Fig. 5.1 it is clearly evident that the energy distance between the S 3p valence band and the Ti 3d conduction band increases, with progressing opening of a band gap. The band gap opening has already been theoretically predicted and experimentally found for several intercalated compounds (see Tab. 5.1). Calculations of single MX_2 layers [40] and of layered compounds expanded in the **c** direction as intercalated but with no guest atom in between [82, 212] also predict this effect. The reason is the decreased orbital overlap along the **c** axis. The width of the S 3p and Ti 3d bands (including crystal-field splitting) are expected to shrink. As already noted, the Ti 3d DOS in Fig. 5.3 is not significantly modified by intercalation. Calculations predict that in particular the two S $3p_z$ states decrease their dispersion. Relative to the bottom of the Ti 3d bands, they have a broader shift than the S $3p_{x,y}$ bands. This is actually observed in Fig. 5.3. According to the interpretation given by Weitering [90] peak B has a larger S $3p_{x,y}$ contribution, while peaks C and D should have mainly S $3p_z$ character. With Na deposition peak D becomes sharper, and both peaks C and D show a larger shift towards higher BE. The EDC decreases at peak B and below (left of) peak D, while it increases between peaks C and D. A quantitative measure of the density of states is not possible for the He I spectra, also because of the increase of secondary emission. The residual of peak B, remaining in all spectra without shifting may be due to unintercalated domains, or to the less-intercalated second TiS_2 slab. Considering this residual, the gap broadening is actually much larger than the valley between peaks A and B. It cannot be decided easily whether peak B decreases because of a shift of the related states. Apart the p band narrowing, peak D shifts by about 0.4 eV to higher BE relative to Ti 3d, and it evidently indicates a general shift of the S 3p group. If the opening of the gap may already be explained not only with the reduced band dispersion, for the increasing distance between S and Ti states electrostatic effects of different nature can be invoked. First, with the increased intra-layer distance induced by intercalated Na 0.28 more electrons are localized in Ti [40]. Electron transfer from the alkaline host is supposed to charge prevalently Ti atoms, and it should contribute with an additional shift. Thus Fig. 5.3, in which Ti states are taken as reference, stresses the relative positive binding energy shift of S relative to Ti. Finally, the interaction of S 3p orbitals with intercalated Na^+ ions may also lead to a positive binding shift.

Compound	Δ band gap (eV)	Method	Reference
$LiTiS_2$	0.8	Semi-empirical calculation (LCAO)	[73]
$LiTiS_2$	0.7	Self-consistent calculation (LAPW)	[43]
$LiTiS_2$	0.24	Self-consistent calculation (ASW)	[163]
$NaTiS_2$	1.1	Self-consistent calculation (ASW)	[163]
Cs_xTiS_2	0.7	SXPS	[213]
$Fe_{1/3}TaS_2$	1	Self-consistent calculation (ASW)	[214]
$Pb_{1/3}TaS_2$	1.3	Self-consistent calculation (LSW and ASW)	[215]
$Sn_{1/3}NbS_2$	1.0	Self-consistent calculation (LSW and ASW)	[215]

Tab. 5.1 Increase of the gap between the transition metal d and chalcogen p bands in the intercalated compound as difference to the pure host compound

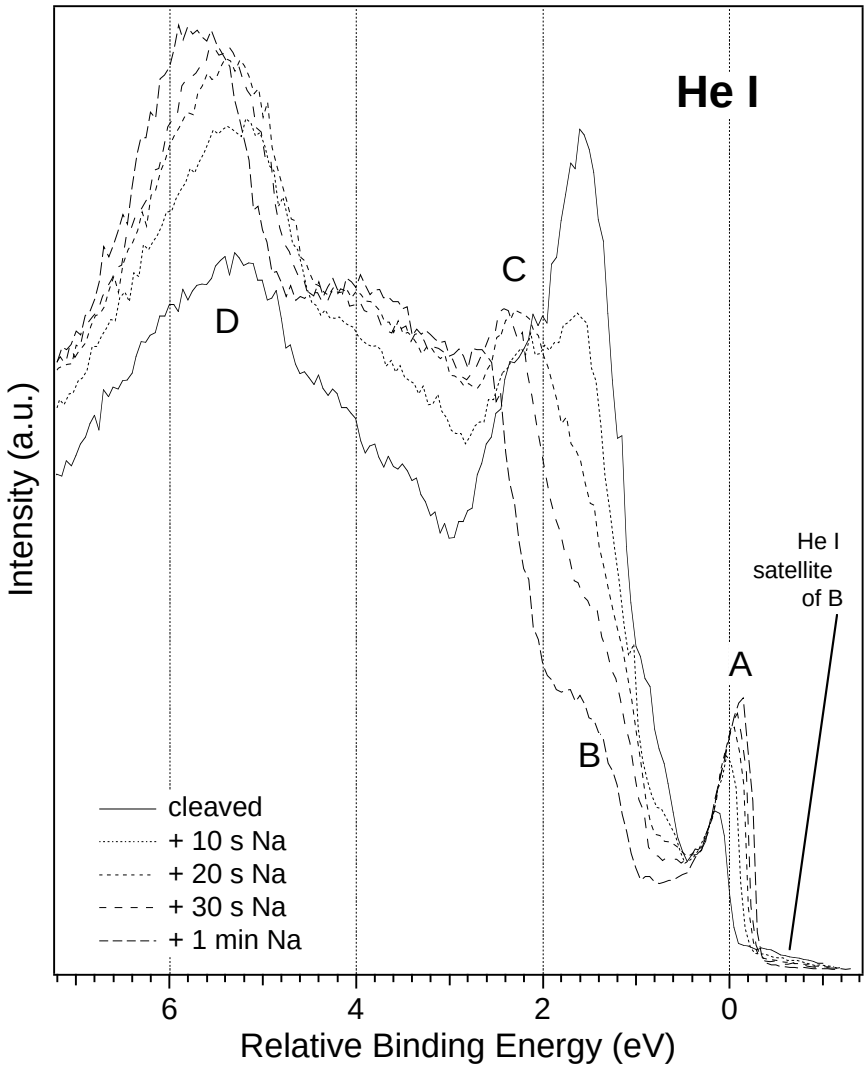

Fig. 5.3 Valence band region for the initial intercalation stages. Spectra have been shifted to match the onset of the Ti 3d band (A): the shift operated to a given spectrum is equal to the BE of its Fermi edge. Letters B-D indicate peaks in the S 3p valence bands

The work function (Fig. 5.4) decreases abruptly with the first deposition step onto the clean crystal. This indicates a dramatic modification of the surface potentials, with probable formation of a surface dipole that would suggest Na adsorption. The decrease progresses more smoothly with further deposition. A time effect is clear with the resting times at Na deposition times of 1 and 16 min, indicating an in-depth penetration of Na and partial restoring of the electronic properties of the substrate. After the initial formation of a surface dipole the work function decreases uniquely due to

the shift of the Fermi level due to the intercalated electrons: by applying exactly the same BE shift as in Fig. 5.3 the secondary cutoff overlaps perfectly, at least for the few initial deposition steps. In this case the work function variation is directly the measure of the variation of the chemical potential of the electrons in the bulk of the intercalated TiS_2 crystal due to the filling of originally empty conduction band states. The work function reported in Fig. 5.4 is a measure of the largest part of the sample surface. With increasing deposition a step grows in correspondence to a fixed work function of 2.88 eV, which is close to the value of 2.75 eV reported for polycrystalline metallic Na [216]. This indicates that a small but increasing fraction of the surface is covered by a metallic Na overlayer.

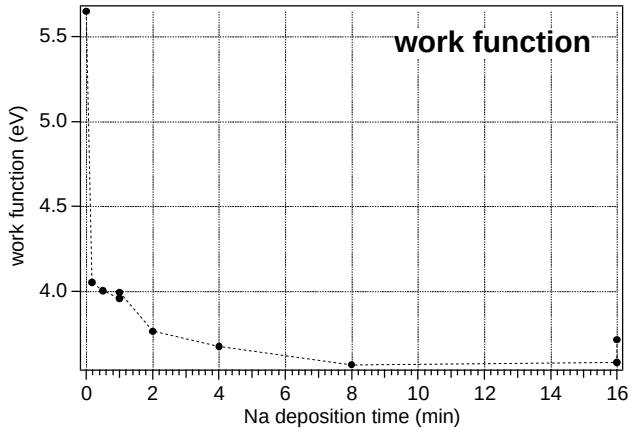

Fig. 5.4 Work function measured from the main secondary emission onset in He I spectra as a function of the Na deposition time

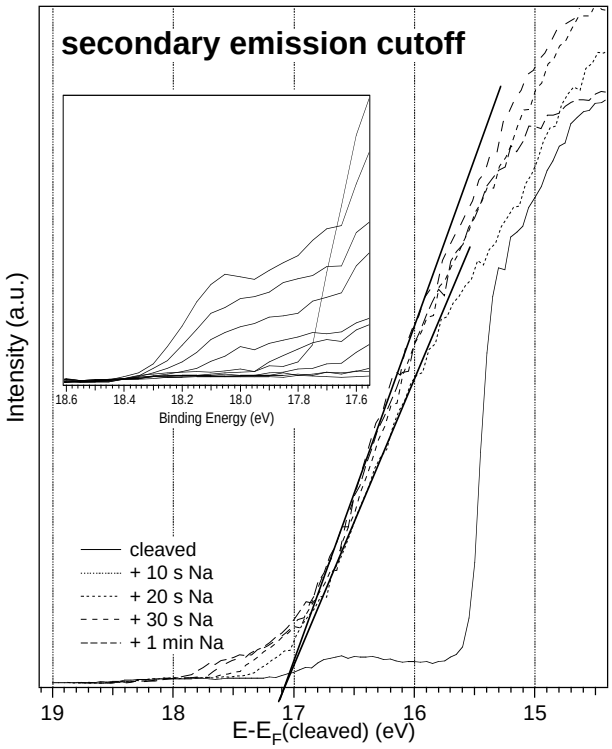

Fig. 5.5 The main secondary emission cutoff of He I spectra with the same shift as in Fig. 5.3. In the inset the lower kinetic energy onset is reported for all spectra shown in Fig. 5.1 (without any shift)

The formation of a metallic Na surface layer is also clear from the comparison of the two strong Na signals: the 1s core level and the KLL Auger line. The latter corresponds to a kinetic energy, which is about 5 times larger than that for the 1s line. As a consequence a larger mean free path (Chapter 2) is obtained, and spectra are much less surface sensitive. With progressing deposition, the intensity of the Auger peaks does not increase as dramatic as for the 1s signal. This suggests that the build-up of Na concentration in the bulk is not as large as on the surface. Both spectra show surface and bulk components. If an alkali ion is also adsorbed on the surface, broader peaks shifted to higher binding energy compared to the same intercalated species are measured [90, 217-222]. This effect can be explained as schematically shown in Fig. 5.7. If alkali are not

intercalated but adsorbed on the surface a strong dipole forms, which is given by the typical large difference in work function (2-3 eV for alkali vs. >5 eV for TMDCs), with electron transfer to the substrate. Na is supposed to intercalate as Na^+-ion, and a similar oxidation state is expected for Na adatoms, as also for most Na compounds as possible surface reaction products. Thus, the measured chemical shift is mainly affected by the local electrical potential drop. Regardless whether Na at the surface exists as adatom or forms hydroxides, we can assign the high BE component to surface Na^+ and the other to bulk (intercalated) Na^+. There may be a contribution of hole screening to the observed binding energy shifts (final state effects) [223]. However, as no reliable estimation of this effect is possible in the present case its contribution is added to the potential drop. The Na KLL spectra show an increasing component located at 260.2 eV, and a much weaker peak at about 262 eV. The assignment to intercalated and surface Na is thus straightforward. It can be noted that the energy splitting between surface and bulk component is initially in the order of 1.6 eV in Na 1s and >2 eV in Na KLL. The dipole value can be deduced from the difference between the work function as reported in Fig. 5.4, and the fixed value of 2.9 eV related to the new surface phase, which may be attributed to metallic Na. This gives a value of about 1.1 eV, which suggests that the chemical shift cannot be considered identical between the two Na forms and that Na at the surface is slightly more ionized than the intercalated. The even larger distance between the two components for the Na KLL signal is due to its higher sensitivity to the chemical shift [138]. Indeed, the decrease of the binding energy difference between the components runs parallel to the change of work function of the substrate.

Up to the *1' Na* deposition step as seen in the He I spectra no surface hydroxide is formed, and also the intensity of the O 1s peaks does not increase dramatically, but the Na 1s peak increases nearly 3 times: this is a clear indication that Na resides on the surface in the form of adatoms or clusters, but not in the reactive metallic form. The comparison of the two signals at different surface sensitivity shows very well that at the first deposition step Na is mainly adsorbed on the surface, but with further deposition steps Na penetrates into the bulk and the surface amount shows only a small increase. With further deposition the surface component increases dramatically and dominates in the Na 1s spectra. At this point, the Auger signal reveals several additional components, indicating that Na exists in various forms, presumably on the sample surface. Whereas the shoulder at 265 eV belongs to the structure of intercalated Na, the broad peak between 263 and 264 eV can be associated to surface NaOH. The formation of this compound is not surprising, as Na accumulates on the surface also in a metal-like state. Moreover, with the largest deposited amount (+ 8 min Na) the Auger spectrum shows a component at 259 eV, which has to be related to the formation of metallic Na. Its characteristic Na KLL BE is 3.5-4 eV lower than for the oxidized forms [138]. The

Na layer acts as a getter on the residual gases, and after prolonged permanence in UHV the Auger spectra return to the shape measured before.

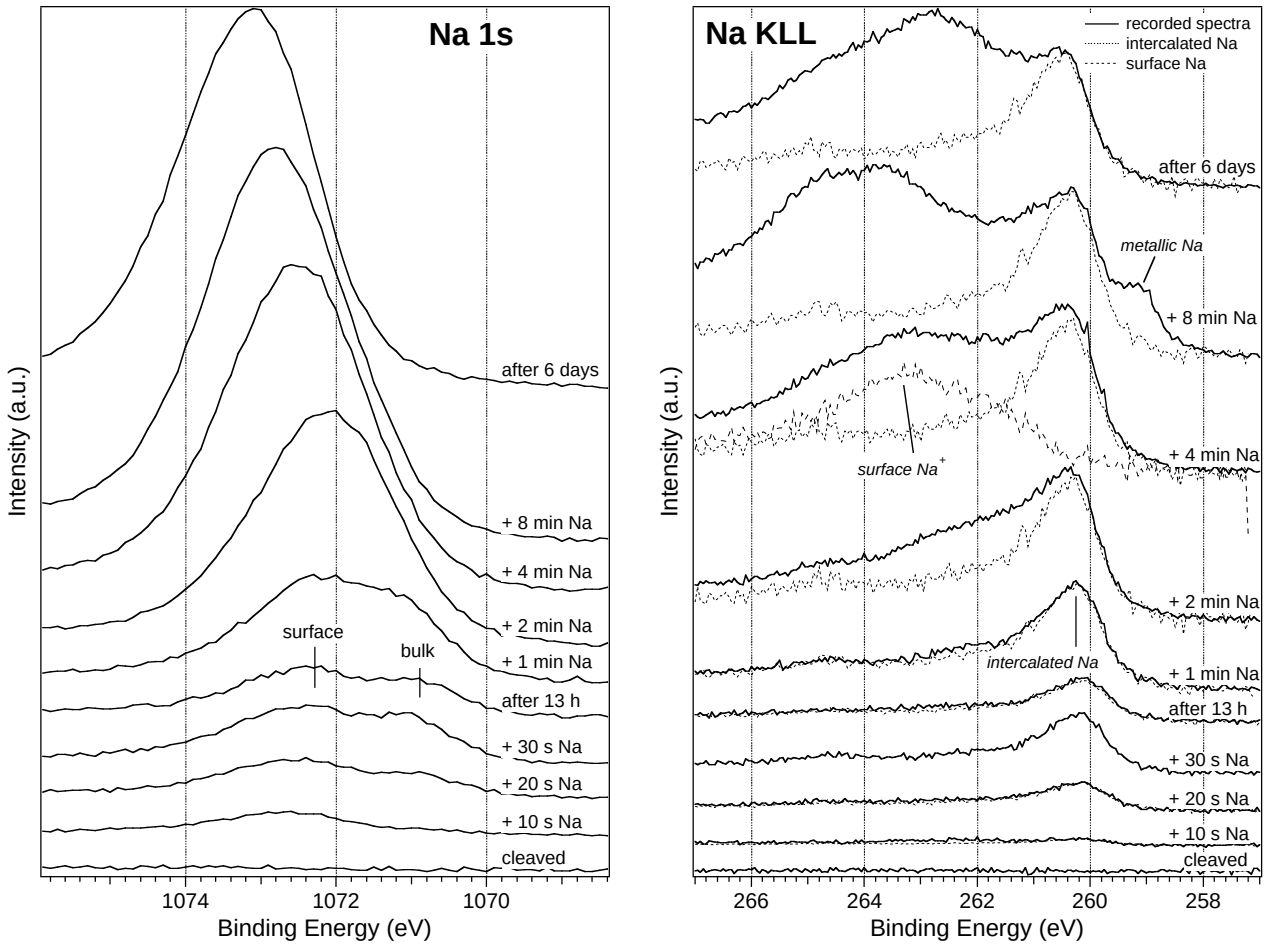

Fig. 5.6 Comparison between the Na 1s core-level and Na KLL Auger emission of a TiS_2 crystal at increasing Na deposition times. The Na 1s signal indicates that after the fourth Na deposition (+30 s) the bulk component has the strongest intensity, as compared to the surface. Given its lower surface sensitivity, the corresponding Na KLL spectrum has been considered as representative of the purely "intercalated" component. This spectrum has been used, shifted and re-scaled to deduce the intercalated component in the remaining spectra here shown. The difference spectra obtained were assumed to correspond to "surface Na"

From this comparison it is clear that the total amount of intercalated Na that typically is calculated from the 1s peak must always be verified with the Na KLL spectra. Since changes in the bulk electronic structure of the substrate depend only on the intercalated amount, a value based on the intensity of the Auger peak at 260.2 eV has to be used in presence of surface species. The mean intensity ratio between the Na KLL and 1s signal for the same Na amount results to be 0.55±0.05, as deduced from other experiments where only Na intercalation was found. The deposition dependence of the intercalated Na concentration determined from the Auger spectra, compared to the apparent total Na concentration is represented in Fig. 5.8. The amount calculated from Na KLL spectra represents the intercalation stoichiometry *x*. It is seen that, due to Na diffusion further into

the bulk, *x* approaches exponentially the maximum intercalation degree of 1 often reported in the literature for TiS_2 [224, 225]. Such a high saturation value has not been reported in the literature, for samples intercalated by deposition so far (see also §2.2.3, and the discussion in §5.1.2 below). If no further Na is deposited (points at 1 min and 16 min), it slowly diffuses into the bulk, and the intensity of the surface sensitive spectra decreases with time. All PES signals have a partial recover with time to a lower *x* value.

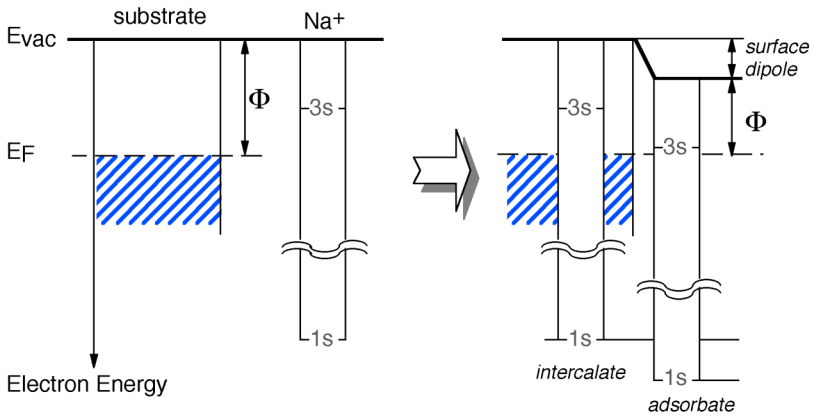

Fig. 5.7 Core level shift observed with in an element present both in the bulk and on the surface of the sample. If the chemical shift due to the oxidation state is identical, the shift corresponds to the surface dipole formed between substrate and adsorbate

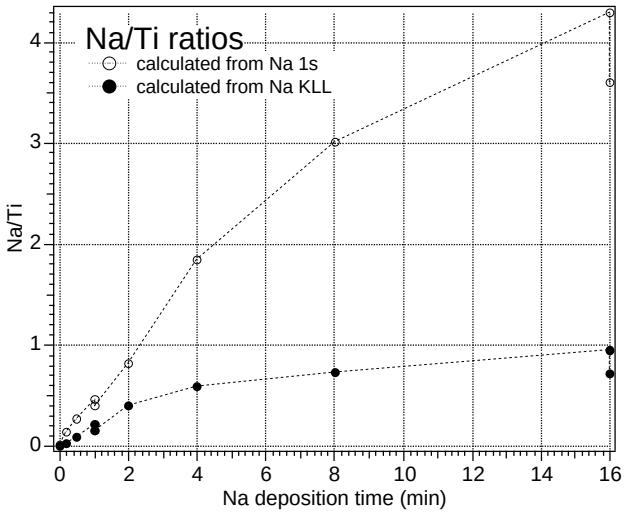

Fig. 5.8 Na/Ti ratios as calculated from the integrated intensity of Na 1s and of the intercalated component deduced from the Na KLL spectra

In Fig. 5.9 core level XPS spectra of the substrate lines are reported. A principle difficulty for the detailed interpretation of the peak shape may arise from presence of domains or staging and different intercalate concentration. The S 2p signal of the cleaved crystal shows nearly no spin-orbit splitting, indicating a strongly heterogeneous chemical environment for the S atoms. The splitting is visible after Na deposition. A one-component fit can satisfactorily be applied only to the last spectra, corresponding to the maximal Na-intercalated compound. A 2-component fit can explain the shape of the initial compound much better. The peak clearly results from two doublets split about 0.6 eV to each other. With the intercalation compound $Fe_{1/4}TiS_2$ Martinez *et al.* observed a 1.2 eV higher BE component has been in the S 2p line. They assigned this second component to

sulfur atoms interacting not only with host Ti but also with guest Fe [226]. In a similar way it can be assumed that the low BE peak corresponds to S interacting with the "regular" 3 coordinating Ti atoms only, while the high BE corresponds to S interacting also with an additional Ti or a Na ion. The difference between the two chemically different guests is not large enough to allow a reasonable 3-component fit within this energy resolution. The increase of the high-BE component at the expenses of the low-BE one is thus well explained by the increasing Na concentration in vicinity of S atoms. This assignation is further supported by two observations at the first deposition step, where Na is essentially only adsorbed. Both the large increase of the high BE component, and the large work function decrease suggest a direct interaction Na-S. Also in ref. [47] a new component is noticed at a higher BE (about 1 eV), and is explained as an interaction with Na, but the influence of a disordering related to the changes of layer stacking is also suggested. Both S peaks tend to shift to higher BE. This shift agrees with most literature, and can be easily related to the shift of the Fermi level induced by the filling of initially empty conduction-band states.

Also for the Ti 2p signal measured for the cleaved crystal a 2-component fit seems to be appropriate. Nevertheless, there is a less clear evidence for the evolution of the components with Na deposition. The two components show a different trend: the high BE peak broadens and shifts to 400 meV larger BE, while the low BE component has a shift to lower BE and remains unchanged in its FWHM. The Ti 2p broadening has been observed also with 3d metal intercalation and has been explained as a final state effect due to additional screening by the itinerant electrons injected in the conduction band [60, 90]. But some authors have argued that an initial state effect may be responsible, due to the inequivalent Ti positions relative to the intercalated atoms [226]. The 2-component fit may suggest a further initial-state based interpretation. Considering the broadening of the high-BE component the intensity ratio does not increase dramatically. In an angle-resolved photoemission study Starnberg *et al.* found both localized and itinerant states contributing to the occupied Ti 3d band of non-stoichiometric TiS_2 [227]. The low-BE component in the Ti 2p signal of the clean crystal is associated to such defect states, as its constant FWHM suggests. The high-BE component shows strong broadening, which should be associated to the increased delocalization and metallic properties induced by intercalation. In particular the 2p and 3p core-hole lifetime of first-row transition metals is decreased by super-Coster-Kronig Auger transitions [164]. This process involves electrons of the metal 3d states, and although they should already be present in pure TiS_2 in small concentration (due to partial hybridization with S 3p states), their amount is greatly enhanced with intercalation. The relative increase of the low-BE component may indicate the formation of further defects with the Na insertion in the vdW gap. In the last spectrum a shoulder at 458.2 appears and was not fitted. The position is in the typical range for TiO_2 [138], the

hydrolysis product of TiS_2 [207] that may be formed by direct reaction with rest gas atoms, or more likely, with the H_2O on top.

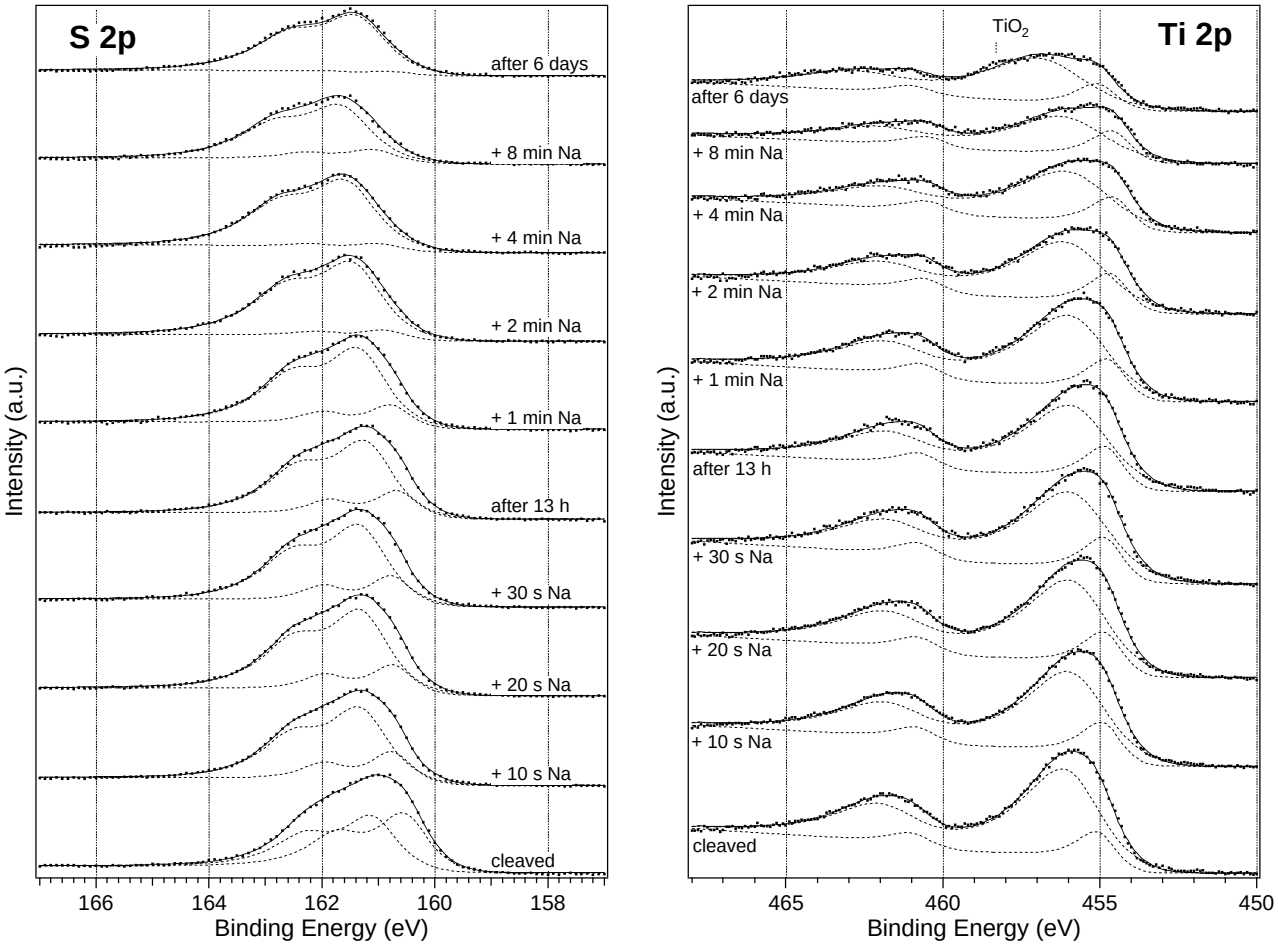

Fig. 5.9 S 2p and Ti 2p XPS spectra of a TiS_2 crystal at increasing Na deposition times (thicker dots) and a 2-component fit (solid line). The two fit components are shown as dashed lines

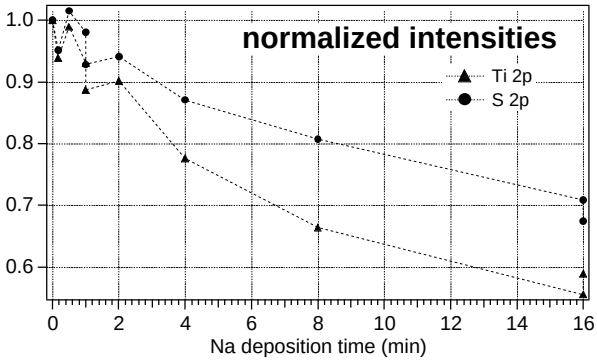

Fig. 5.10 Normalized values of the integrated peak intensities for the substrate core levels as function of the Na deposition time

The Ti and S substrate core-level intensities decrease at different rates with Na deposition (Fig. 5.10). The intensity of the Ti 2p signal decreases faster than that of the S 2p. This is due to the formation of the surface overlayer, which affects more the signal with a lower kinetic energy (shorter mean free path of the electrons and higher surface sensitivity). Thus the relative stoichiometries given for non-homogeneous specimens may be affected by severe systematic errors.

The intensity variations with the rest time after the last deposition (16 min) may be explained as a reorganization of the surface Na layer to islands and parallel formation of TiO_2 surface contaminations.

5.1.2 Na/$TiSe_2$

Published experimental results of Na intercalation into $TiSe_2$ appeared only in ref. [228]. The aim of this work was to demonstrate the deintercalation of an alkali metal, if an electronegative and oxidizing reactant was adsorbed on top of the intercalated crystal. No systematic Na deposition series have been investigated. Only an optimal amount of Na was deposited onto $TiSe_2$ to prepare the intercalated phase. For $TiSe_2$ only the Se 3d spectra are reported, which shows a shift to higher BE.

He valence band spectra can be assigned in analogy with TiS_2 (Fig. 5.11). Although $TiSe_2$ is a semimetal [40], no occupied Ti 3d band is visible proving that this crystal is not self-intercalated. It has been reported that synthesis of stoichiometric compounds is easier for $TiSe_2$ than for TiS_2 [229]. Nearly no surface contamination features appear even after prolonged deposition. The full-range He I spectra (not reported here) also do not show contribution of adsorbed O-species. The evolution of the substrate core-level lines and their intensity evolution (Fig. 5.12) also suggest that no overlayer is formed. After an initial fast decrease in the Ti 2p and Se 3d intensity a nearly constant level is approached which shows some variation depending on the deposition sequence. The O 1s XPS signal remains below the detection limits. The two shoulders at left from peak D appeared after resting times. A close examination of the Se 3d spectral shape indicates a slight change in the intensity ratio of the spin orbit doublet at the same steps, and a tiny shoulder at 54.8 eV (see Fig. 5.18 below). This suggests the formation of a small amount of oxidized Se, but a convincing mechanism cannot be given. Due to the lower Se electronegativity, the B-D group is at lower BE than for the corresponding sulfide. The energetic extension is narrower than in TiS_2, according to theoretical calculations [40]. Also in this case the Ti 3d band is clearly filled upon intercalation, and similar trends are observed with bands B-D. However, changes are less dramatic. In particular the band gap does not clearly open within the maximum Na concentration that could be obtained in this experiment. This Na amount (see below) is approximately the same as for the last spectrum of Fig. 5.3. This contrasting tendency is in nice agreement with calculations of Fang *et al.* [40]. They found that when taken as a single slab, TiS_2 becomes a semiconductor, while $TiSe_2$ should remain a semimetal.

The smaller decrease of the work function with Na indicates that in this case no Na adatoms and related surface dipoles are formed. Also no other steps in the secondary emission cutoff are evident, as found for TiS_2. This further proves a more easy penetration of Na into the bulk of $TiSe_2$.

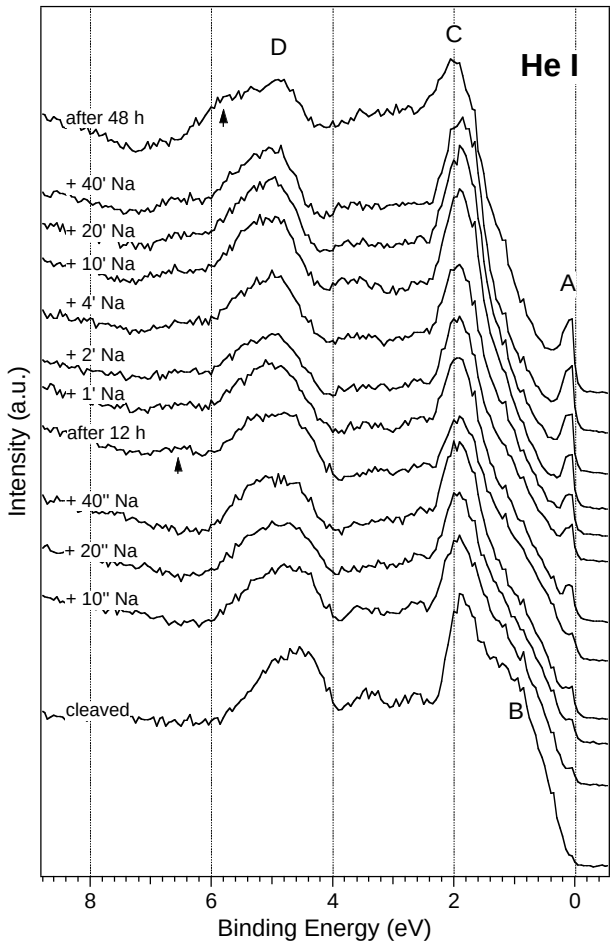

Fig. 5.11 Valence band spectra measured with an excitation energy of 21.2 eV (He I) on a cleaved $TiSe_2$ crystal after depositing increasing Na amounts or after resting times. Arrows indicate features that appeared after resting times

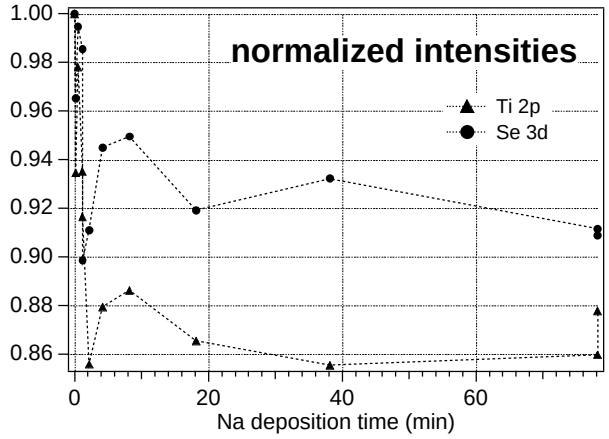

Fig. 5.12 Normalized values of the integrated peak intensities of the substrate core levels as function of the Na deposition time

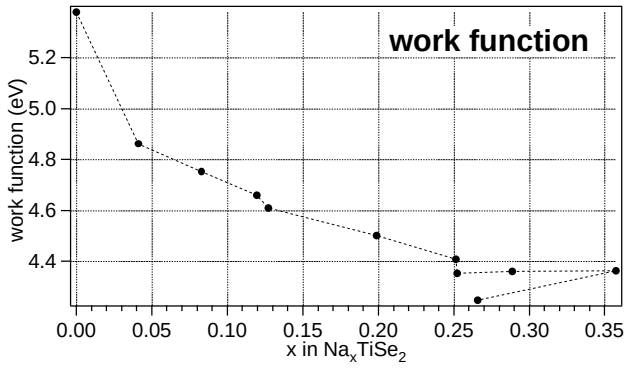

Fig. 5.13 Work function measured from the main secondary emission onset in the He I spectra as a function of the Na concentration

Compared to TiS_2 the Na 1s signal is much narrower, and no other components other than intercalated Na show up in the Auger KLL spectra. Thus the Na/Ti ratio calculated from the Na 1s and Ti 2p peaks appears a reliable measure of the intercalated Na concentration *x* in this case. The evolution of the Na concentration as function of the deposition time is shown in Fig. 5.15. This typical profile was observed with any alkali dispenser independently from its previous operation time. Therefore a simple effect of decreasing evaporation rate can be excluded. A similar profile was reported also by Bronold *et al.* [37] for SnS_2 intercalated with K or with Na. In this paper also an initial "induction period" was observed, where the alkali XPS intensity had little increase with deposition time. This was attributed to a low initial sticking coefficient. No induction period was observed in the present work. A possible cause is that only semimetals or metals were investigated and not semiconductors like SnS_2. This would indicate that some phenomena in UHV deposition depend on the electronic properties of the substrate.

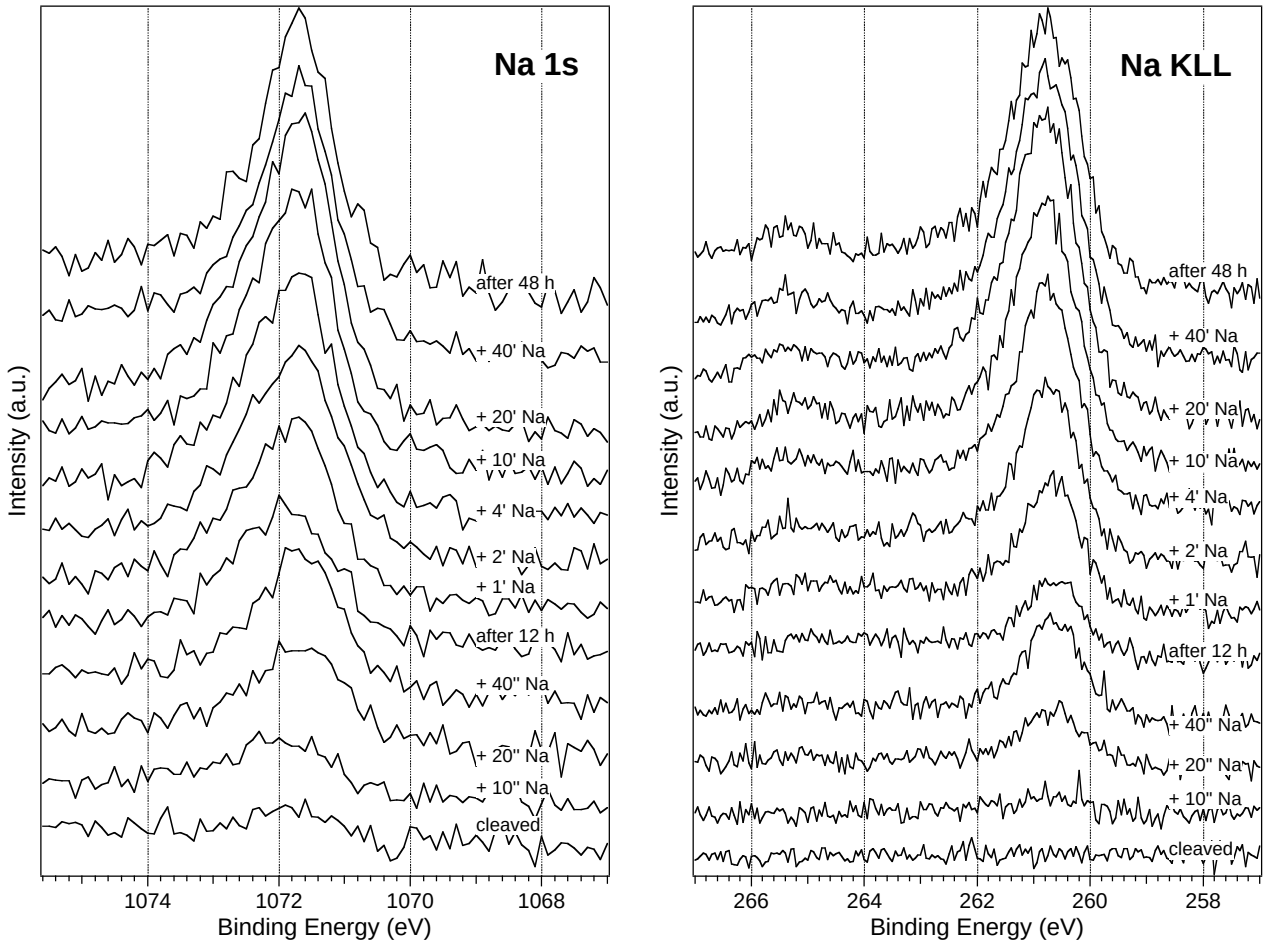

Fig. 5.14 Na 1s core-level and Na KLL Auger emission of a $TiSe_2$ single crystal in the course of the Na deposition experiment

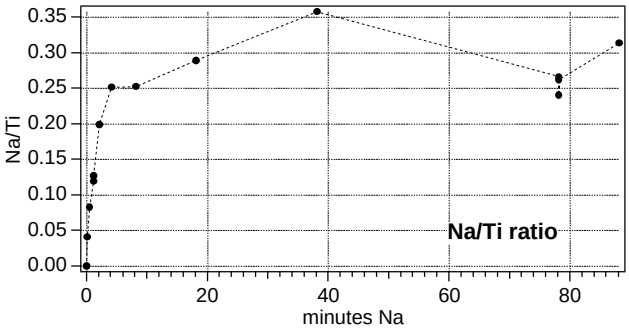

Fig. 5.15 Na/Ti ratios as calculated from the integrated Na 1s intensity as function of Na deposition time on a cleaved $TiSe_2$ crystal

As already pointed out in §2.2.3, also in the literature always a limiting value of the guest/host ratio was reported. As an example the following compositions have been attained by deposition of alkali metals: $Na_{0.5}SnS_2$ and $K_{0.33}SnS_2$ [37], $Na_{0.1}WSe_2$ [230], $Na_{0.3}TaS_2$ [218], $Na_{0.3}VSe_2$ [221], $Na_{0.1}VSe_2$ [91], $K_{0.3}VSe_2$ [91], $K_{0.5}WS_2$ [27], $Cs_{0.6}TaSe_2$ [217], $Cs_{0.2}ZrSe_2$ [213], $Cs_{0.2}VSe_2$ [91]. With Li tendencially higher stoichiometries are obtained [231]. The scatter and inconsistency even for the same system was already noticed by Bronold *et al.* [37], and indicate that possibly also the experimental conditions and in particular the substrate morphology and stoichiometry are of importance.

For an explanation of this effect we can assume a constant information depth of the XPS signal, and a constant alkali metal sticking coefficient (and thus a constant intercalation rate). We can explain the exponential evolution of the *x* value (Na/Ti ratio) if we exclude that the guest is evenly distributed in the whole crystal, but that intercalation proceeds at a front instead (Fig. 5.16). Within the shallow, near-surface region of the crystal, which can be observed with XPS, the guest concentration is increased only to a limiting value. Afterwards, with continued deposition only further diffusion into the bulk is achieved without changing the near-surface composition, and little or no changes are observed in XPS spectra. The formation of an intercalation front has been observed with RBS in both directions across and along the layers for Hg/TiS_2 [232] and Ag/TiS_2 [233]. Layer by layer intercalation has also been shown using dynamic high resolution transmission electron microscopy (DHRTEM) for $(NH_4^+)(NH_3)_y$ intercalation into 2H-TaS_2 [234]. The concentration saturation cannot be caused by a decreasing sticking coefficient of the alkali metal on the substrate. The previous experiment of Na deposition on a largely self-intercalated TiS_2 crystal demonstrated that even metallic layers could be obtained under similar conditions. On the other hand, even when metallic layers could be obtained by low-temperature deposition no evidence of definitely higher concentrations has been found [90].

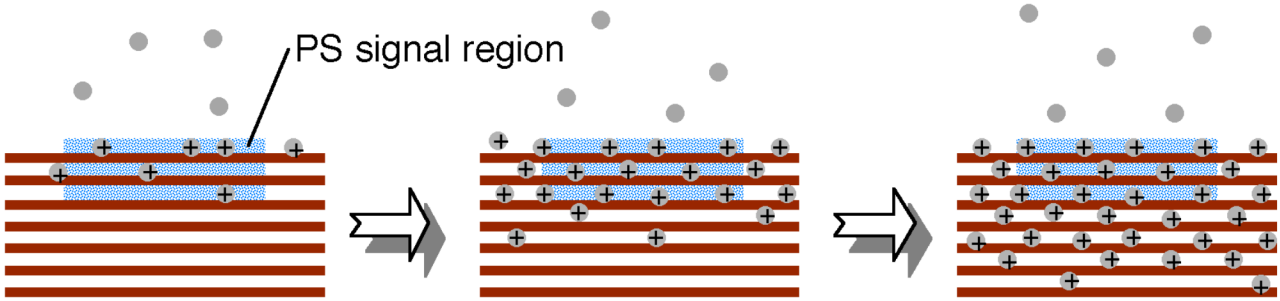

Fig. 5.16 Scheme for the formation of an intercalation front. As a consequence a limiting intercalate concentration is observed with PES

The limiting concentration seems to be related to a system-specific, well-defined composition, which is determined by kinetic and/or energetic factors. As already mentioned in §2.2.3, Bronold *et al.* attributed this behavior to the existence of a diffusion barrier for the alkali ions [37]. A diffusion of Na into deeper-lying van der Waals gaps is energetically favorable for the system if at a particular composition further increase of x leads to the occupation of less favorable sites by the guest species. For small values of x the site energy should be nearly concentration independent due to negligible Coulomb interactions among the intercalated cations, which may become more important when particular superstructures of the intercalated guests are approached. In electrochemical intercalation the existence of voltage plateaus without phase transitions has been observed at characteristic alkali concentrations [235]. An explanation in terms of ordering effects induced by a repulsive Coulomb interactions has been given [94, 95, 235, 236]. Approaching the critical concentration of x=0.25-0.3 the partial molal entropy drops by more than an order of magnitude [237], thus increasing the free energy of the intercalated compound. An alternative explanation for the existence of a limiting concentration may be strain induced within the slabs during their glide induced by Na intercalation. Intercalated Na prefers a trigonal prismatic coordination, while initially only tetrahedral and octahedral are available (§2.2.1). Weitering and Hibma found evidences based on electron diffraction measurements, that these strains may form defects in the slabs [90]. Such defects would then allow a faster intercalation into the bulk. Not independent from these considerations is a kinetic interpretation based on the Na chemical diffusion coefficient in TMDCs. As shown in Fig. 5.17 the diffusion coefficient increases with x. At the initial intercalation level diffusion is very low and Na accumulates rapidly. If the local concentration increases, also the mobility increases. Unless high deposition rates are reached, it will not be possible to accumulate Na at higher concentration. Further aspects of the mechanism of intercalation will be discussed also on the basis of the results of the co-deposition experiments in §5.2.3).

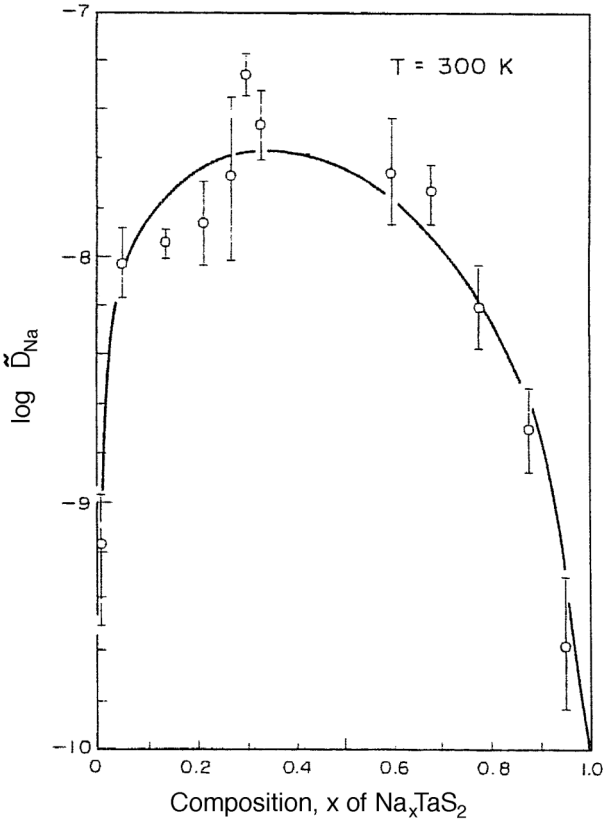

Fig. 5.17 Dependence of the chemical diffusion coefficient of intercalated Na in dependence of Na concentration. Taken from ref. [30]

The same clear Na 1s and Na KLL signals were found also for all other investigated single crystals, suggesting that the intercalation behavior is not sensitive to the non-identical presence of morphological defects, which may vary from sample to sample. The phenomenology reported with the Na/TiS_2 system represents an exception which is related to the high degree of self-intercalation of the specimens used. The high alkali concentration found in the TiS_2 experiment can be explained by a slower diffusion related to an increased lattice stiffness induced by interstitial Ti. This may hinder the formation of appropriate sites in the van der Waals gap for Na diffusion. The negative effect of self-intercalation on the Li diffusion coefficient in TiS_2 was already recognized in the early works on Li batteries and was attributed to the pinning of the slabs [30, 168].

Se 3d spectra of $Na/TiSe_2$ are shown in Fig. 5.18. Also the evolution of the calculated fit parameters in a one-component fit is reported. Differently from S 2p in Na/TiS_2 a one-component fit was satisfactory in this case. The intensity attenuates continuously as function of the deposited Na amount and it is taken as the independent variable. With this choice the graphics indicate a higher Na concentration by progressing leftwards. Also in this case the asymmetry parameter α tends to more negative values with intercalation. The asymmetry with increased intensity at the high BE side of a core-level line is related to the excitation of hole-electron pairs near the Fermi level during the photoemission process. A higher DOS at E_F (i.e. larger metallicity) leads to a larger asymmetry [165, 166, 238, 239]. The FWHM increase is correlated with a decrease of the G/L

fraction. The latter parameter indicates the fraction of the Lorentzian broadening from the total spectral broadening. It may be argued that the core hole lifetime remains unaffected by intercalation, and that increased broadening is dominated by Gaussian nature. This suggests that instead of formation of a well-defined new component, the interaction with vicinal Na^+ ions creates an increasing number of inequivalent Se sites. If compared with the previous Na/TiS_2 system the fits of the chalcogen core levels obtained there suggest a different Na-chalcogen interaction. In the case of TiS_2 Na seems to occupy fixed interstitial positions, while in $TiSe_2$ Na may be rapidly hopping between different sites, so that each Se may see an envelope of different possible environments. This view is consistent with the faster Na penetration in the bulk that is observed with the $TiSe_2$ crystals.

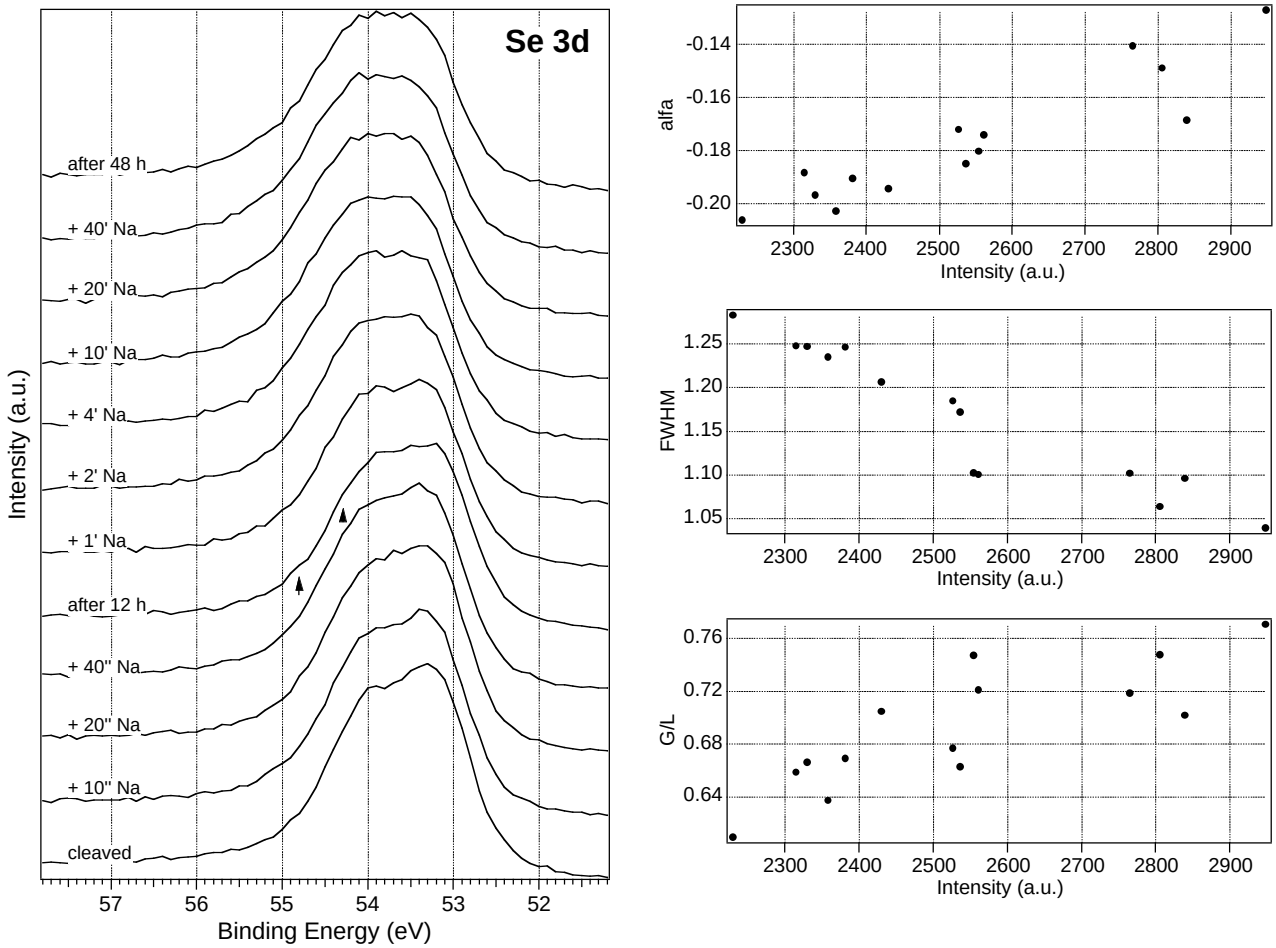

Fig. 5.18 Se 3d XPS spectra of a $TiSe_2$ crystal at increasing Na deposition times. Arrows stress the increased component after the experimental resting time. On the right side a correlation is shown between fitted Se peak intensity and α, FWHM, and Gauss/Lorentz parameters

The Ti 2p signal (Fig. 5.19) is narrower than in the case of TiS_2, and clearly indicates a larger homogeneity of the pristine host compound. The most evident feature with intercalation is a strong broadening. The broadening of the Ti 2p peak has already been reported for TiS_2 intercalated with Na, K, Ag [90] and 3d metals [60]. As in this case no relevant contribution of interstitial Ti is

present, a single component fit is possible. It reveals no clear evolution of the binding energy with the Na content. As for Se 3d α tends to more negative values by progressing with intercalation, and the total FWHM increases linearly while the peak intensity decreases. The broadening may be related to the already discussed super-Coster-Kronig effect [164]. The missing BE increase could be explained by the screening induced by electron transfer to itinerant Ti 3d states. This screening would compensate the shift of the reference E_F level due to intercalation. For host concentrations of 0.2-0.4 in TiS_2 other authors proposed a 2-component fit, instead [60, 90, 226]. They assigned the lower BE component to better-screened Ti, either in the initial or in the final state. A 2-component fit, with the same number of free parameters as in the one-component could also be applied with good agreement with experimental data (Fig. 5.19 right). However, in the cited references fits are only executed for a well-defined concentration, and the high-BE component is interpreted as the new feature that appeared after intercalation. In the fit, applied to the present composition-dependent study, it is clearly seen that instead the high-BE component develops at the expenses of the low-BE instead. This trend cannot be easily justified, but the shifts agree to those found in Na/TiS_2. Considering that Ti atoms occupy positions perpendicular to the Na sites, a direct interaction Na-Ti may be responsible for the high-BE component. An initial state effect due to inequivalent position of Ti in relation to the intercalated metal was already proposed by Martinez *et al*. [226]. In that case the metal was Fe, and a direct interaction between *d* orbitals was suggested. But as the Ti 2p broadening is similar with different guest species, including alkali [90], it cannot be specifically related with a chemical interaction with the guest.

Although both fits appear formally correct and to some extent explainable, for its simplicity the one-component fit appears preferable. With this assumption the fact that with self-intercalated TiS_2 two components were necessary must then be related uniquely to the presence of inequivalent Ti already in the host compound, which behave differently with intercalation.

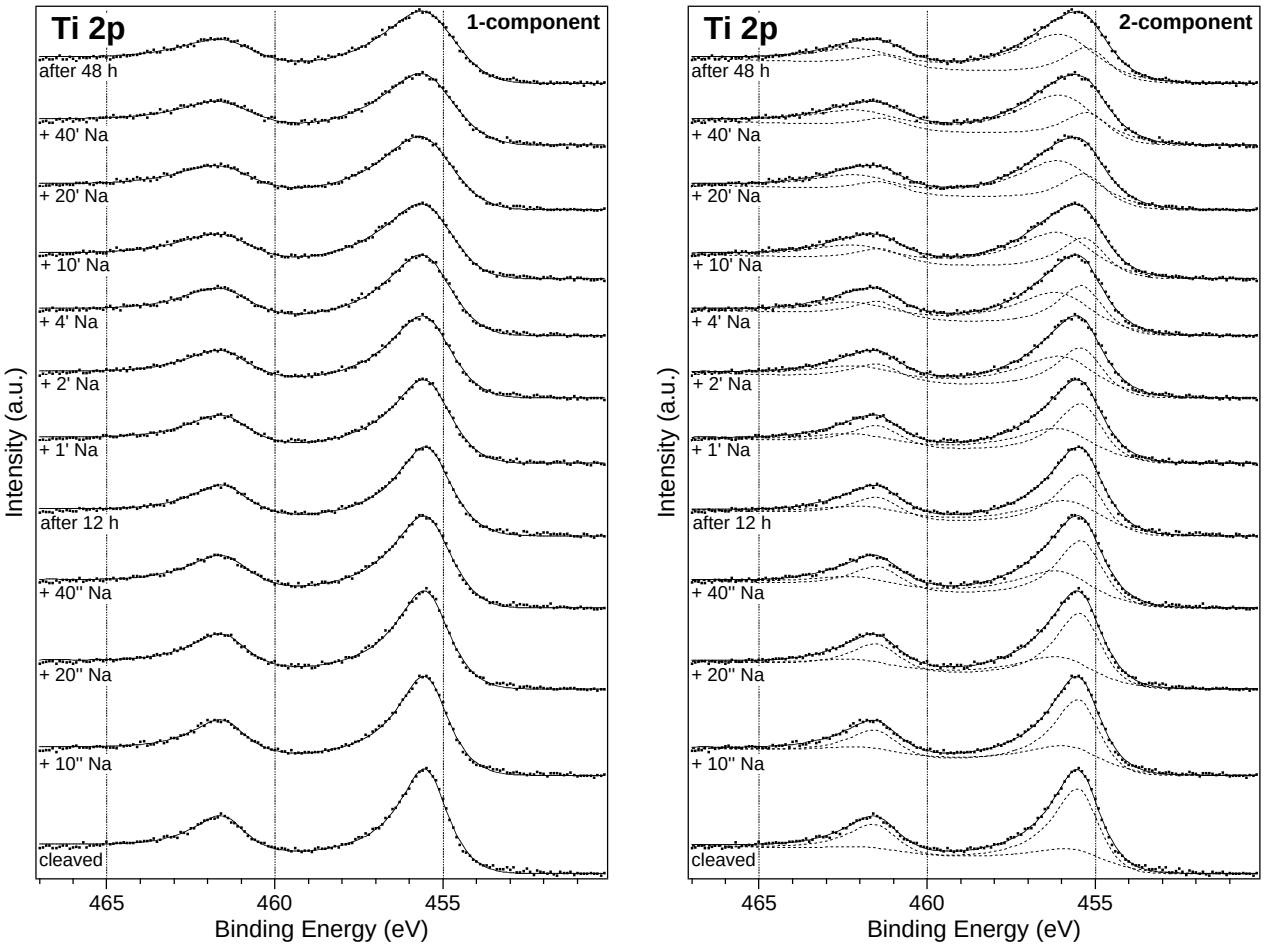

Fig. 5.19 A comparison between a 1- and a 2-component fit for Ti 2p XPS spectra of a $TiSe_2$ crystal at increasing Na deposition times (thicker dots). Fit results are shown as solid lines and components as dashed lines. In the 2-component fit only intensities and BEs were fitted, while the asymmetry factors were forced to the same value

5.1.3 Na/1T-TaS_2

This system has been studied by PES [218, 219, 240]. In ref. [218] Na is deposited at a temperature of 150 K. Even at this temperature no metallic Na overlayer forms on the surface, but only disordered, nearly ionized adatoms are formed. After annealing to RT the ratio Na/Ta is estimated to be 0.25. The Ta 5d-derived occupied states shift to higher BE with the opening of a band gap at the Fermi level already for a small amount of intercalated Na. The valence-band S 3p states are shifted to higher BE, whereas the Ta 4d line is shifted to lower BE. The largest shift is observed for the Ta 5d states and is explained as an electron localization effect in the intercalated compound.

As already anticipated, Na reaches a limiting concentration also on TaS_2 as on $TiSe_2$ (Fig. 5.20). The Na spectra have a similar evolution, showing the same nearly constant binding energy and the lack of any chemically shifted line (compare Fig. 5.14). This suggests that this kind of intercalation behavior is not very sensitive to the kind of chalcogen or transition metal in the host.

The saturation concentration does not depend on the electronic properties, either: TaS_2 is a metal as also the self-intercalated $Ti_{1+x}S_2$ used for this series of experiments, but it behaves like the semimetal $TiSe_2$.

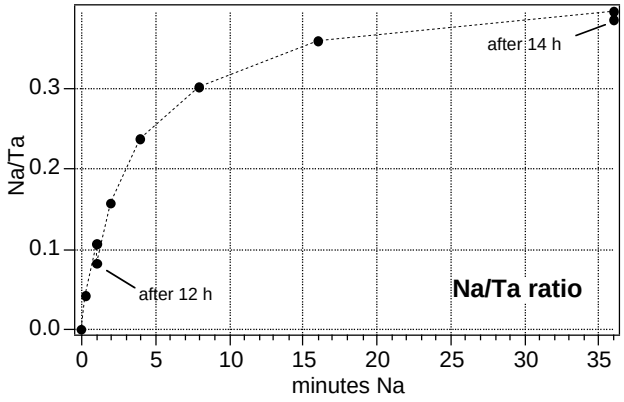

Fig. 5.20 Na/Ta ratios as calculated from the integrated Na 1s intensity vs. the Na deposition time on a cleaved 1T-TaS_2 crystal

TaS_2 has 1 electron in the Ta 5d band, and valence spectra show a high density of states at the Fermi level for the pristine crystal (Fig. 5.21). Apart this difference, the photoemission peaks can be assigned in analogy to the TiX_2 systems. Due to the d electron in the valence band the E_F position relative to the S 3p bands is energetically higher than in TiS_2. Therefore, all emission lines have higher BEs. With intercalation band A becomes more intense, and the maximum tends to shift to higher BE. The electronic density at the Fermi level decreases drastically, as a consequence of the filling of the conduction band with electrons transferred from Na. As is indicated by Fig. 5.20, the largest Na increment occurs after the *2 min* deposition step. After this step the band width of A decreases, but no evident gap opens between the Ta 5d states and the S 3p states. There may be some indication of a small gap opening formed at the Fermi level as previously found with SXP spectra [217, 231]. The opening of the gap cannot be explained as the complete filling of the d_{z^2} band, since this would require the intercalation of 1 equivalent of Na, considering a complete charge transfer. Because of the CDW localization in 1T-TaX_2 compounds peak A is composed by three sub-bands, of which only the one at highest energy has states to be filled. The DOS of this band corresponds to 1/13 of the total Ta atoms, and it is filled with just the equivalent small amount of intercalated Na. The main changes for peaks B-D are similar to those observed for TiX_2 and may be explained within the same frame. As a difference, peak D shows no narrowing and appears to be slightly broadened instead. Therefore the decreased band dispersion is possibly masked by a splitting of this band into two components.

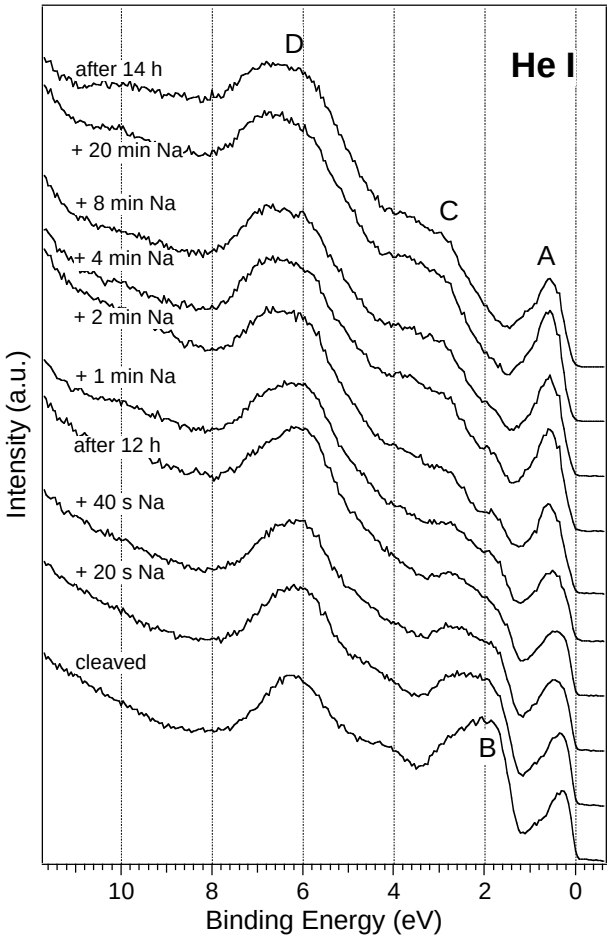

Fig. 5.21 Valence band spectra measured with an excitation energy of 21.2 eV (He I) on a cleaved 1T-TaS_2 crystal after deposition steps of increasing Na amounts or after resting times

As a consequence of the charge density waves in 1T-TaS_2, different equivalent Ta positions will result with different chemical shifts (§2.1.2). Charge density waves are very sensitive to the atomic and electronic structure. LEED experiments show that several intercalation stages with different CDW are formed with alkali metal deposition on 1T-$TaSe_2$ and 1T-TaS_2 [31, 218, 231]. The different components cannot be resolved by the laboratory equipment used for this experiment, and only qualitatively changes of CDW phases may be evaluated by the peak symmetry. Some more details will be discussed in the section reporting co-deposition experiments studied with SXPS. Thus, no simple shape fit can be attempted with the Ta 4f core level. Also in this case the peaks broaden, but in a much smaller extent than with TiX_2. The main reason is also different: in 1T-TaX_2 the broadening is a sign of increased CDWs, which is an effect of the increased number of conduction electrons. A clear shift of 0.2 eV of the Ta states to lower BE is observed in this case.

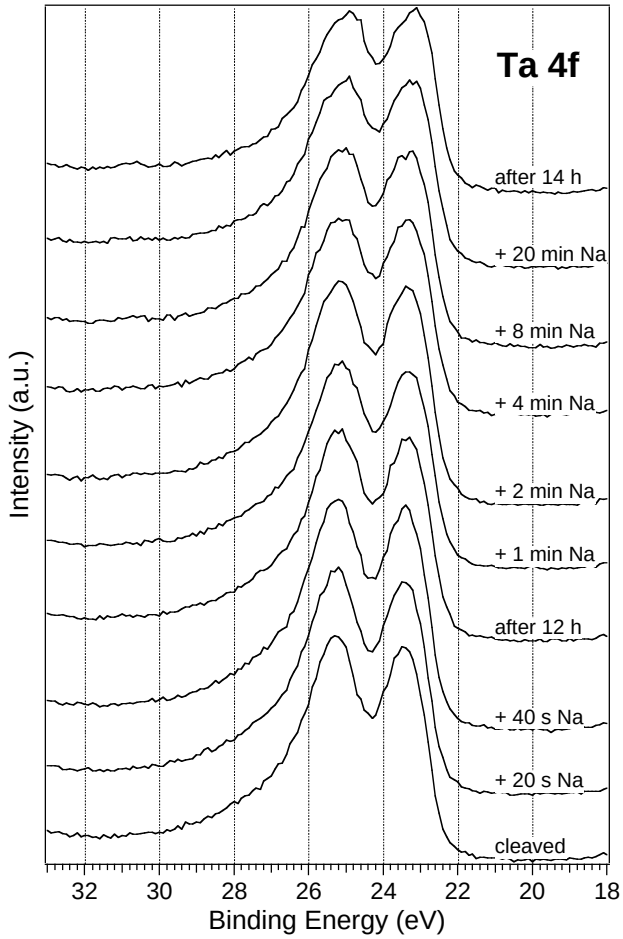

Fig. 5.22 Ta 4f XPS spectra of a cleaved 1T-TaS_2 crystal at increasing Na deposition times

The S 2p doublet could be satisfactorily fitted with a single component (Fig. 5.23), and it was not possible to apply any two-component fit. The main evolution in the peak shape is a progressing broadening with a FWHM increase from 1.02 to 1.15 eV. As for Na/$TiSe_2$, the chalcogen core-level broadening can be explained by the presence of inequivalent S interacting with Na, which is also supposed to be hopping between different intercalation sites. With a progressive, periodic Na occupancy of the interstitial sites 3 new, well-defined components should appear in sequence, since each S atom can coordinate from 0 to 3 Na ions. The peak broadening confirms the S-Na interaction, but also indicates a random distribution of the site occupancies. As with Se 3d, the energetic resolution of the S 2p signal does not allow a reasonable 4-component fit, which could reveal the different coordination numbers and their distribution as function of the Na concentration. A change of this distribution may influence the asymmetry parameter α. However, its decrease with intercalation is clear (see Fig. 5.23). The principal cause appears to be the decrease of the metallic behavior, as is also indicated by the lower EDC(E_F) value in the UPS spectra.

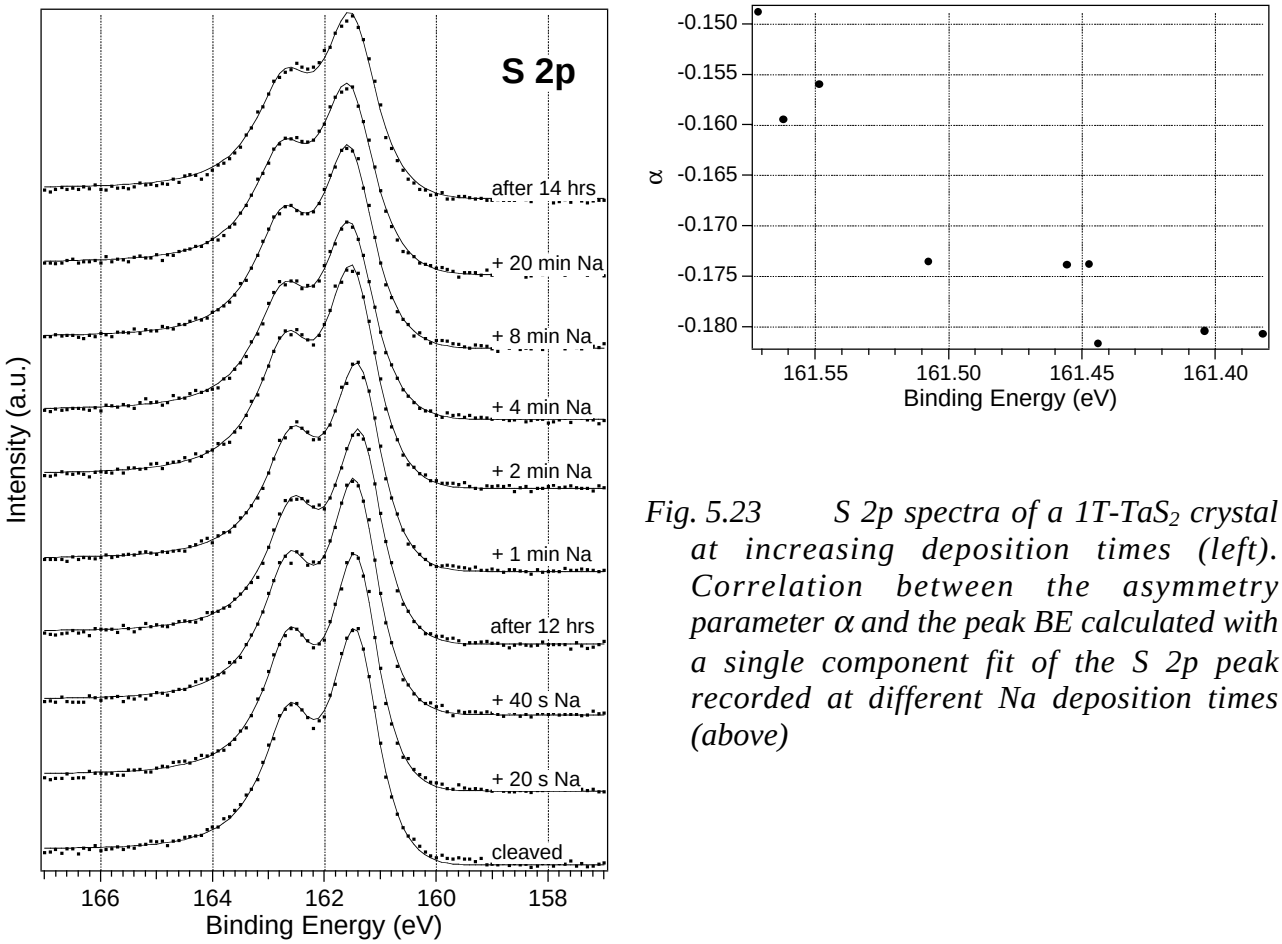

Fig. 5.23 S 2p spectra of a 1T-TaS_2 crystal at increasing deposition times (left). Correlation between the asymmetry parameter α and the peak BE calculated with a single component fit of the S 2p peak recorded at different Na deposition times (above)

5.1.4 Na/1T-$TaSe_2$

1T-$TaSe_2$ has recently attracted large interest because it is known to exhibit a large number of CDW phases in dependence of temperature or intercalation. But no published work of UHV Na intercalation exists so far.

In this case the Na content was found to increase quite steeply to the saturation value, with an abrupt transition between two different regimes, which is related to accumulation in the topmost layers and diffusion into the bulk. This behavior was reproduced by using other crystals of the same batch. This may confirm that intercalation across the slabs requires the presence of defects and that these are created only, when the amount of alkali is such to destabilize the 1T stacking sequence.

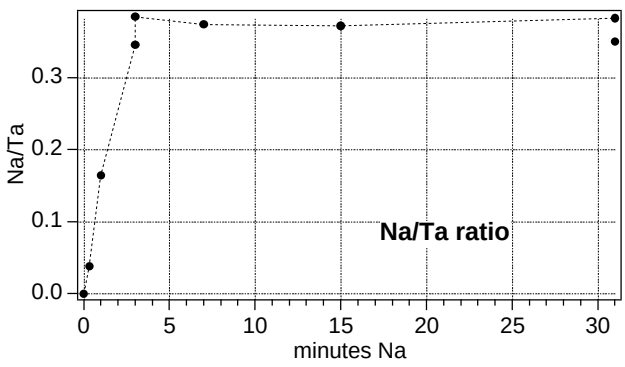

Fig. 5.24 Na/Ta ratios as calculated from the integrated Na 1s intensity vs. the Na deposition time on a cleaved 1T-$TaSe_2$ crystal

The evolution of peaks A-D in the valence band reproduces that of the other systems studied for Na deposition. Changes are larger at the early deposition steps, while after 4 min total deposition nearly no change can be observed any more. Evidently, this reflects the evolution of the Na content. In this case the opening of a gap of about 200 meV between the Fermi level and the top of the valence band is more evident than with 1T-TaS_2, and takes place with the largest Na variation, between x<0.2 and x>0.3. The gap between the chalcogen p bands and the transition metal d bands increases more in the sulfide than in the selenide also with TaX_2 as with TiX_2. More evident than in 1T-TaS_2 peak D broadens and splits into two sub-bands.

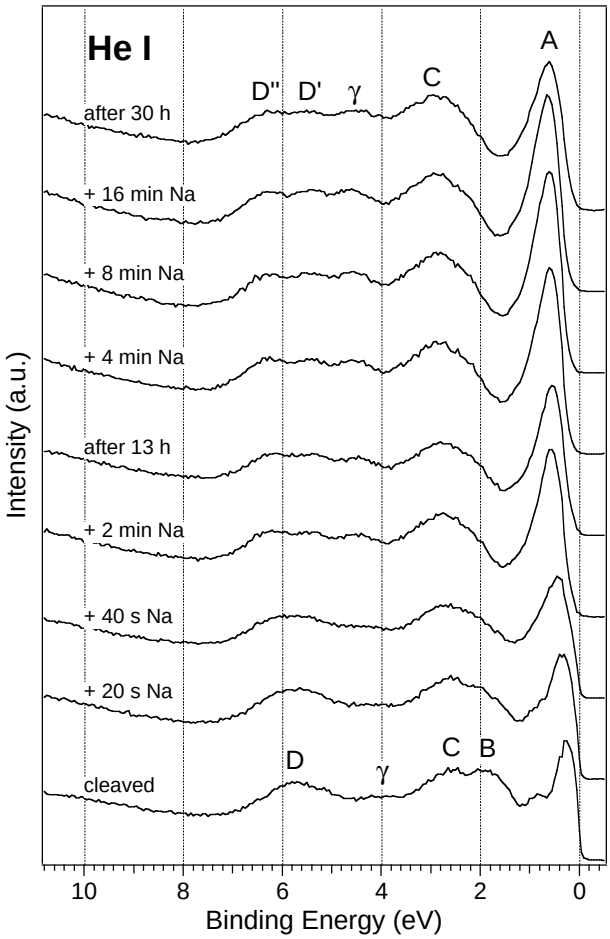

Fig. 5.25 Valence band spectra measured with an excitation energy of 21.2 eV (He I) on a cleaved 1T-$TaSe_2$ crystal after deposition steps of increasing Na amounts or after resting times

The substrate core levels reveal very small changes. By fitting the Se 3d the asymmetry decreases also in this case. As in the other cases Se shifts to higher BE and Ta to lower BE (Fig. 5.25). In 1T-$TaSe_2$ the $\sqrt{13}\times\sqrt{13}$ CDW phase is commensurate, that is the wave phase coherency is found over large domains, whereas in the corresponding sulfide the same $\sqrt{13}\times\sqrt{13}$ phase is said to be nearly commensurate, and extends only in small domains of a few nm. Therefore, the inequivalent Ta positions are better defined, and the splitting is more evident here. The spectral results in comparison to the data obtained with 1T-TaS_2 (see before) clearly indicate the

intercalation of Na into the substrate. The resulting changes in the electronic structure will be discussed later on.

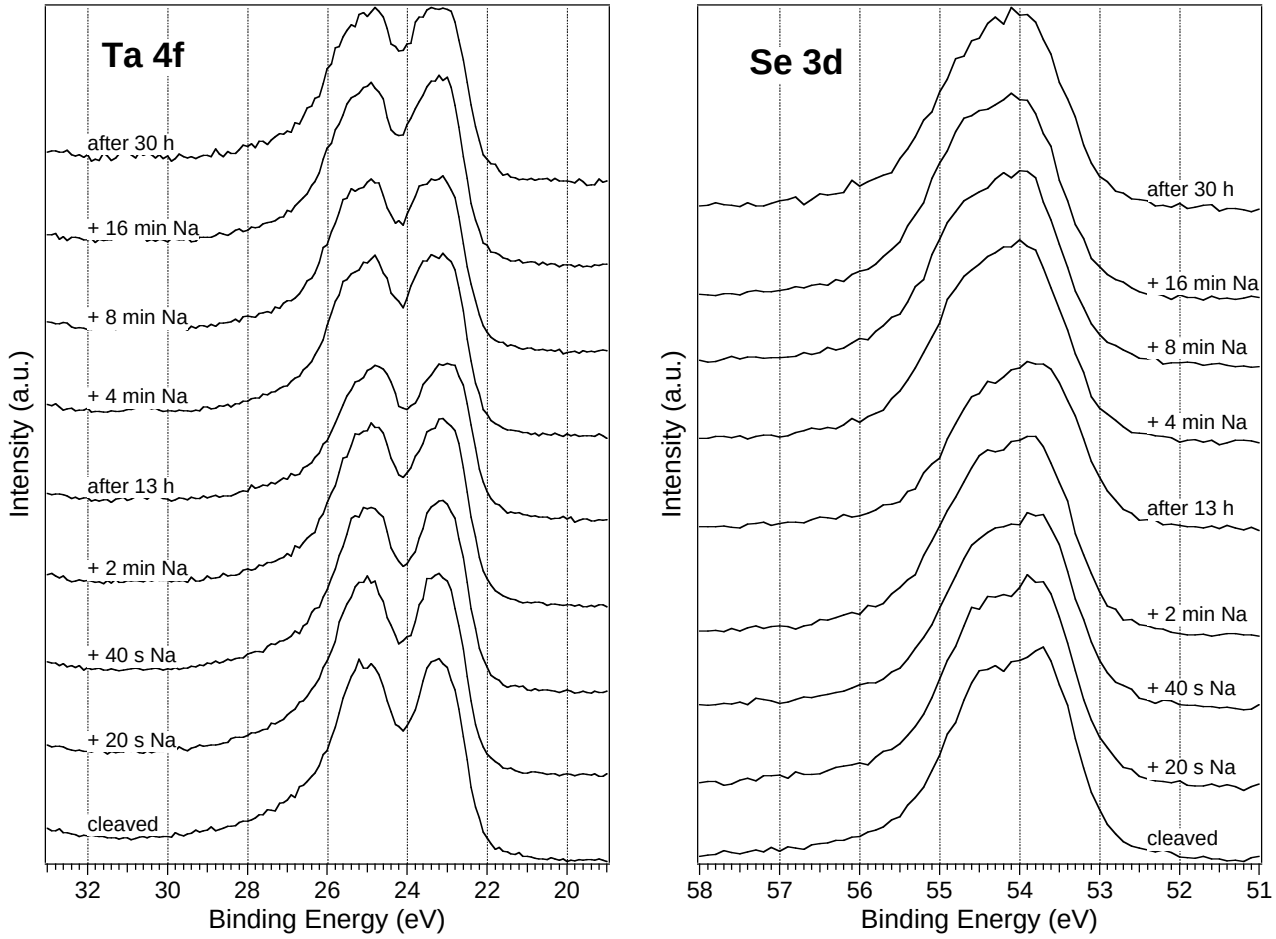

Fig. 5.26 Ta 4f and Se 3d core level spectra on a cleaved 1T-$TaSe_2$ crystal after deposition steps of increasing Na amounts or after resting times

5.2 Co-deposition experiments

With respect to Na intercalation no radical changes could be observed by photoelectron spectroscopy using a set of hosts with different atomic sizes and electronic properties. In this section results on the investigation of the role of the alkali metal will be presented. These results have already been published (refs. [241-246]), and only the aspects that are more relevant to the mechanism of UHV intercalation and its energetics will be described here.

The relative tendency among the different alkali metals to intercalate can be compared directly by deposition of two different alkali in sequence. In a recent work Starnberg *et al.* [222] deposited subsequently Na and K on VSe_2. K was found to remain on the surface of Na-intercalated VSe_2, while the deposition of Na on the K-intercalated substrate forced K to deintercalate indicating the superior stability of the Na-intercalated compound compared to the K intercalated one. In the present work the investigation was extended to the alkali Li, Na, and Cs. In order to evaluate all

core levels this experiment was executed at BESSY with 1T-$TaSe_2$ as substrate. The charge density waves of this crystal are very sensitive to the charge transfer and were used as a further probe to keep track of intercalation.

In the first part the alkali co-deposition experiments will be reported. Further details on the interactions between intercalated ions have been obtained in a similar experiment using co-deposition of an alkali metal and an electron acceptor, that will be presented in the second part. All effects will be discussed in the last part of this section.

5.2.1 Na, Li and Cs/1T-$TaSe_2$

Na/Li/1T-$TaSe_2$

Fig. 5.27 shows the substrate valence band spectra during Li and subsequent Na deposition. The spectra and their changes at the first part of the experiment are similar to those obtained for Na deposition in laboratory studies (§5.1). With Li deposition the topmost peak broadens, the valence band is shifted towards higher binding energies (if referred to the Fermi level), and the electronic density at the Fermi level decreases. A dramatic change of the electronic structure is evident at the last Li deposition step. The new structure is known to correspond to that of 2H-$TaSe_2$ [217]. No further dramatic changes occur with subsequent Na deposition. The Ta 4f signal (also shown in Fig. 5.27) of pristine 1T-$TaSe_2$ consists of a 2 eV-separated doublet (4f 5/2 and 7/2 spin-orbit coupling) at RT, in which both peaks are split because of the $\sqrt{13}\times\sqrt{13}$ charge density wave of $TaSe_2$. In fact, the Ta 5d valence electron is periodically displaced from the electrostatically most favorable (average) position in a star-of-David symmetry [1, 2]. When the electronic density in the conduction band is further increased, due to the electron injection by intercalated alkali, also the splitting in the Ta 4f signal is enhanced. A similar effect has been observed also with other deposited alkali metals. No CDW at RT is observed on 2H-$TaSe_2$ [1], and with the 2H→1T transition the charge density waves vanish and the splitting of the Ta 4f line disappears.

The Li 1s and the Se 3d signals are shown in Fig. 5.28. The Se peak becomes broader with Li intercalation, as already noticed for the Na/$TiSe_2$ system. With the last Li dose, the Li peak becomes much more intense, and mostly covers the Se one. The broadening of the Li 1s line towards higher BE indicates that at least part of the deposited Li remains as adatom on the surface. Due to this coverage of the surface, all substrate intensities are reduced at this step.

When a small Na amount is deposited on top the Li 1s signal is substantially reduced, strongly suggesting a Li penetration into depths exceeding the electron free mean path (about 7 Å for the kinetic energy corresponding to Li 1s electrons irradiated with 80 eV photons; as a consequence practically only ions intercalated in the first van der Waals gap are detected). The

substrate intensities do not increase significantly, indicating that the Li sites are occupied by Na ions.

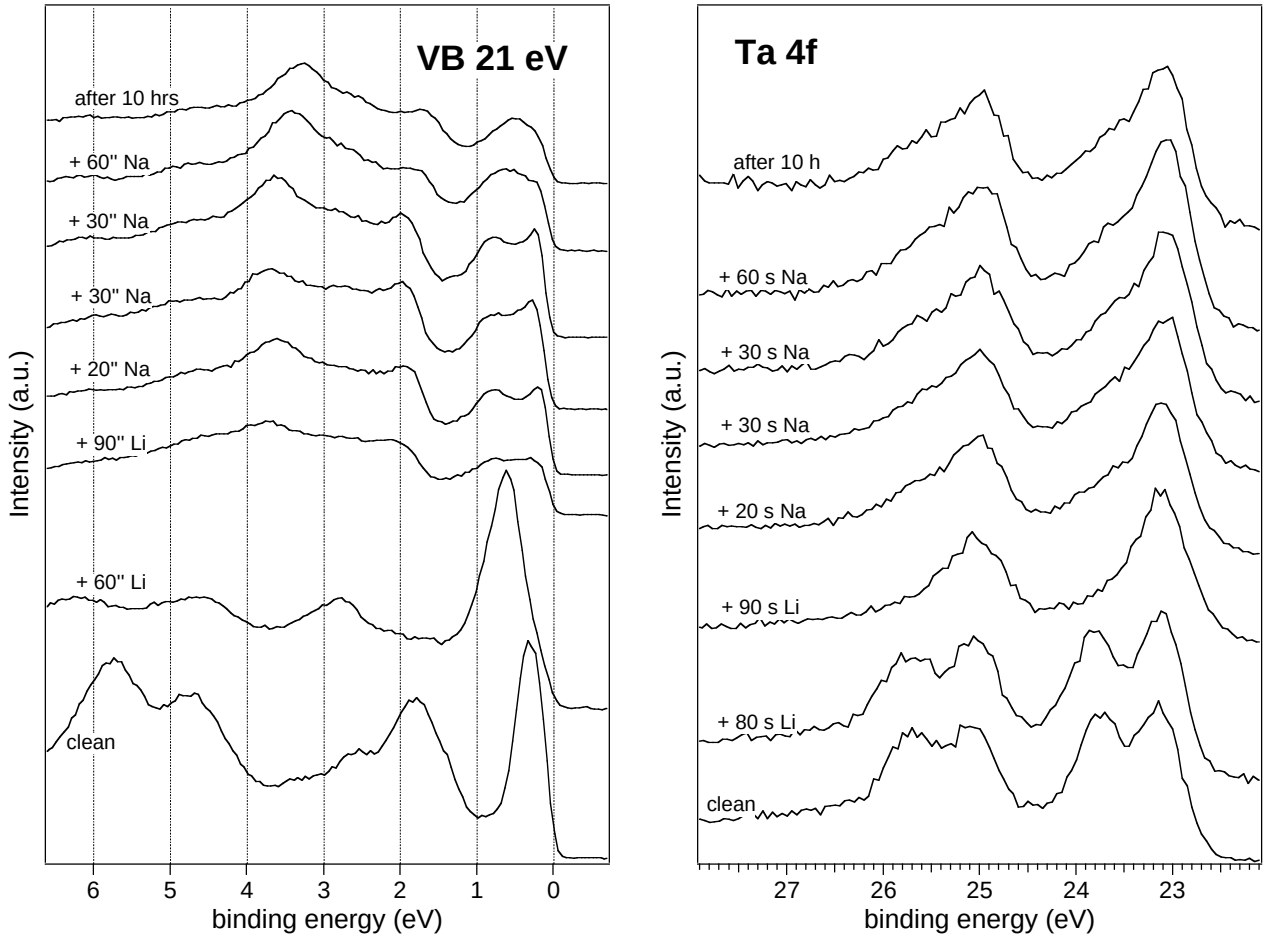

Fig. 5.27 Valence band spectra excited with hν=21 eV (left) and Ta 4f core-level emission excited with hν=80 eV (right) for a cleaved 1T-$TaSe_2$ crystal, and after Li and subsequent Na deposition steps

Na 2p (Fig. 5.28) is found to increase progressively with increasing doses. The broad peak is a clear sign that Na is mainly adsorbed on the surface. With the last spectra measured, the effect of over 10 hours resting time is also shown: the Li peak is slightly decreased compared to the Se signal. Also the Na intensities are found to decrease compared to the substrate. With a similar experiment repeated on TiS_2 (not shown) evidence for Na both adsorbed on the surface and intercalated were more clearly evident from the measured spectra.

No other alkali than Li, even deposited for much longer time, was found to lead to the 1T→2H transition. Also the Ta 4f peak shape is significantly modified only with Li deposition. This is certainly due to the higher intercalation ratio *x* which typically can be reached with Li in these type of UHV *in-situ* experiments ($x \approx 0.9$, according to Crawack [231]), because in principle also Na is able to induce the 1T→2H transition [67].

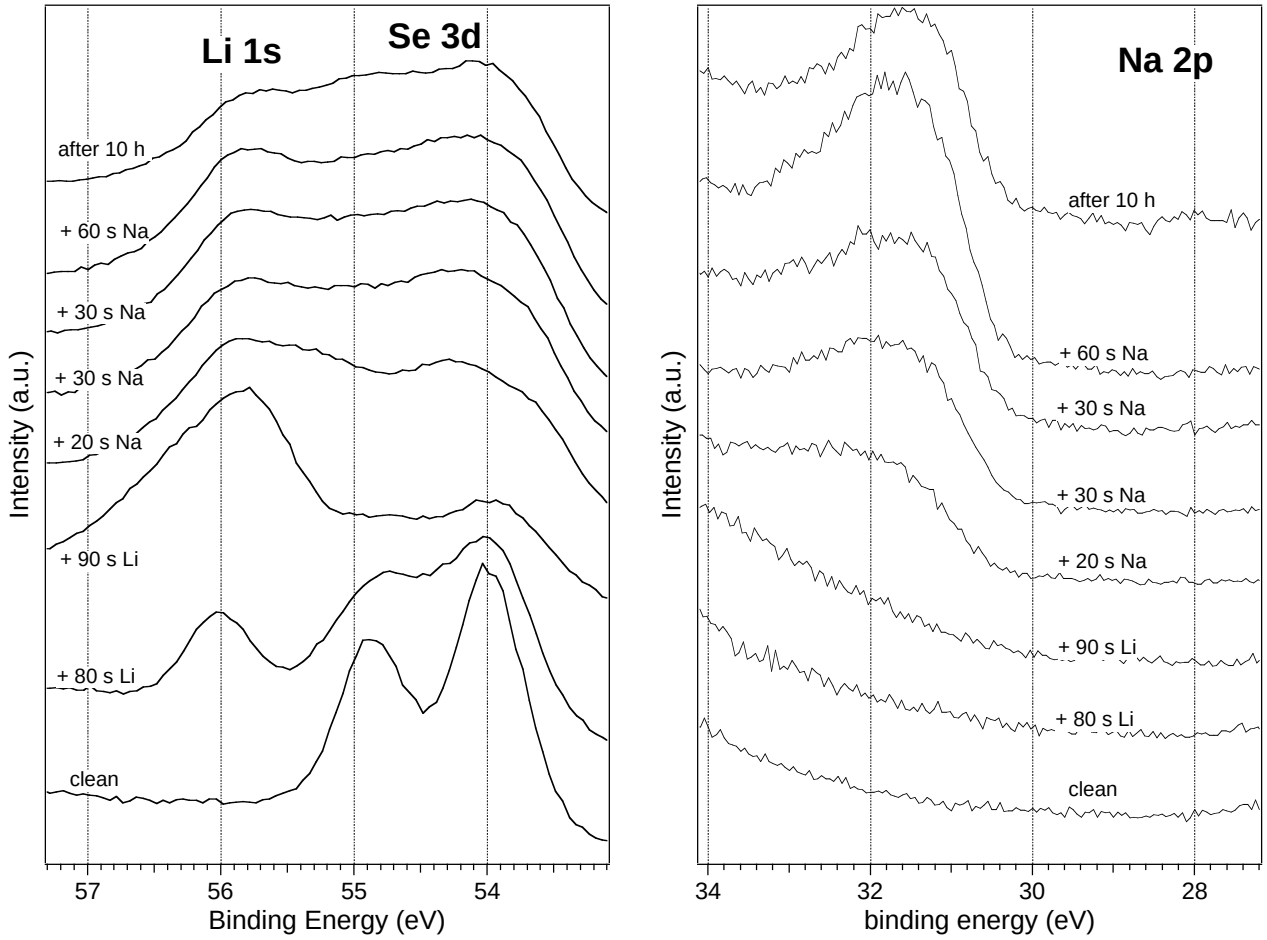

Fig. 5.28 Li 1s, Se 3d and Na 2p core-level emissions excited with hν=80 eV of a cleaved 1T-$TaSe_2$ crystal, and after Li and subsequent Na deposition steps

Li/Na/$TaSe_2$

When Na is deposited before Li, the symmetry of the CDW splitting changes already for smaller Li doses (Fig. 5.29). This indicates that even if always deposition of Li atoms is necessary for the phase transition, after Na deposition the 1T phase is already destabilized by a higher electron density in the conduction band states. By increasing the electron density in the conduction band even further with Li deposition, at first the CDWs are changed, and finally the 2H phase results as the most stable configuration. Also in the case of intercalated Na on cleaved $TaSe_2$ the characteristic broadening of the Se 3d peak can be observed.

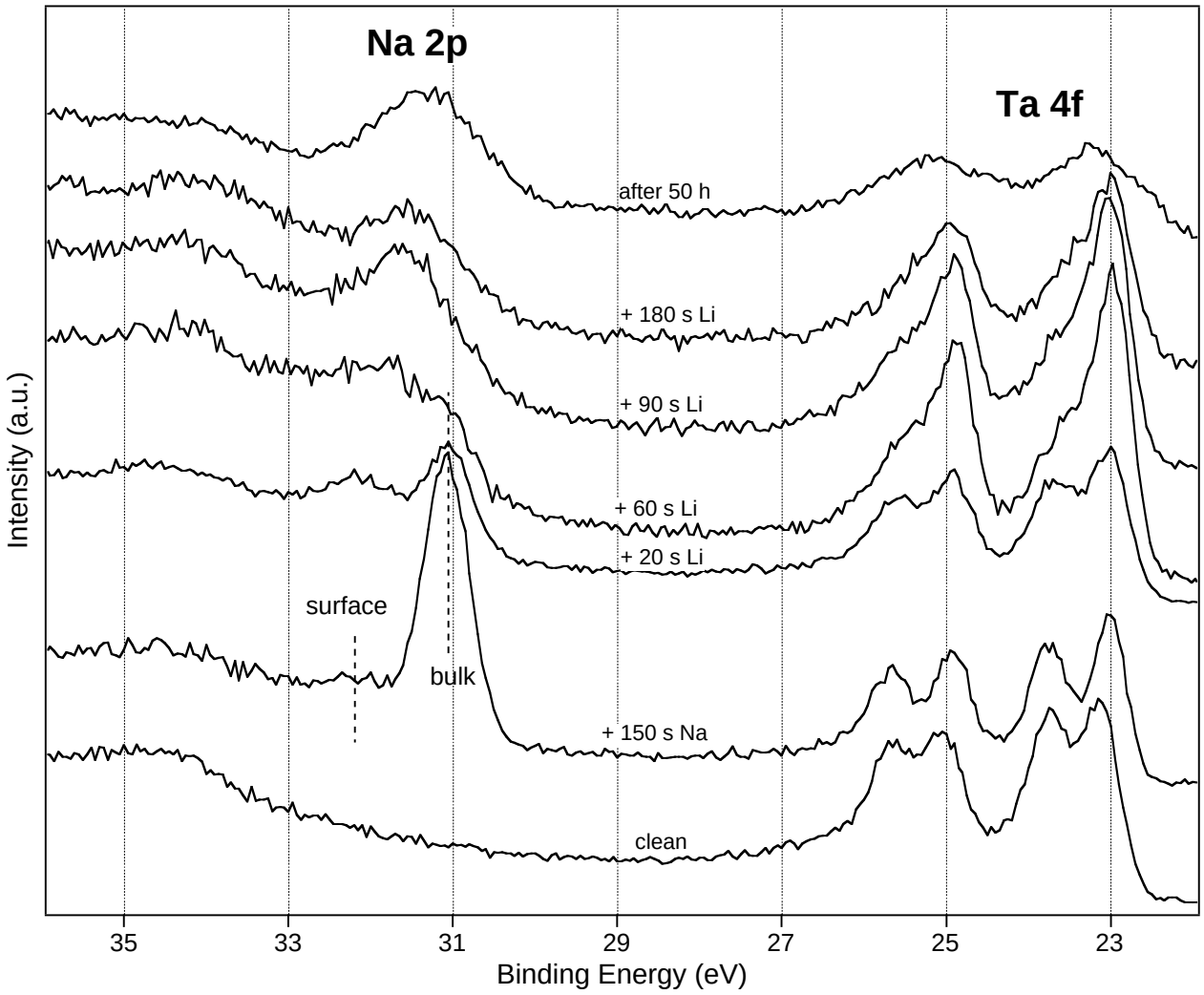

Fig. 5.29 Ta 4f and Na 2p core-level emissions excited with hν=80 eV for the cleaved 1T-$TaSe_2$ crystal, and after Na and subsequent Li deposition steps

In the Na 2p spectra (Fig. 5.29 left) two components coexist, a sharp low-BE and a broad high-BE component, which are attributed to the surface adatom and bulk (i.e. intercalated) Na species. Li deposition on a Na-intercalated substrate leads to a dramatic decrease of the intercalated component, while the higher-BE shoulder increases until it dominates the spectra. After the strong decrease with the first Li deposition, the total area of the two peaks remains almost unchanged with subsequent steps. Most of the initially intercalated Na is evidently pushed deeper into the bulk. From the second Li deposition the spectra indicate that part of the remaining surface-near Na is pushed back to the surface by co-deposited Li. With time Na slowly continues to deintercalate, covering the substrate. After 50 hours the Na 2p peak is much stronger and broader, while the Ta 4f line becomes much weaker. Li penetrates deeper into the bulk: its 1s emission line, which clearly develops in intensity during Li deposition, is found to decrease compared to the Se 3d after the *50 h* resting time.

Cs/Li/TaSe₂

On the Li-intercalated $TaSe_2$, Cs is found at first not to intercalate, but only to remain adsorbed on top, as indicated by the comparison of the binding energy of the 5p peaks (Fig. 5.30 right) with previous experiments [217]. Only with much larger Cs amounts deposited an intercalated component is visible at lower binding energy, as indicated by the arrows. On the other hand Li is repelled by the Cs overlayer: its 1s signal decreases compared to the Se 3d one (Fig. 5.30 left) which indicates its penetration into the bulk of the substrate. The effect of the 1T→2H phase transition on the Se 3d is clearer in this experiment than in the one shown in Fig. 5.28. After the *+ 90 s Li* step two doublets indicate the coexistence of the two phases. With time and Cs deposition only the 2H component remains.

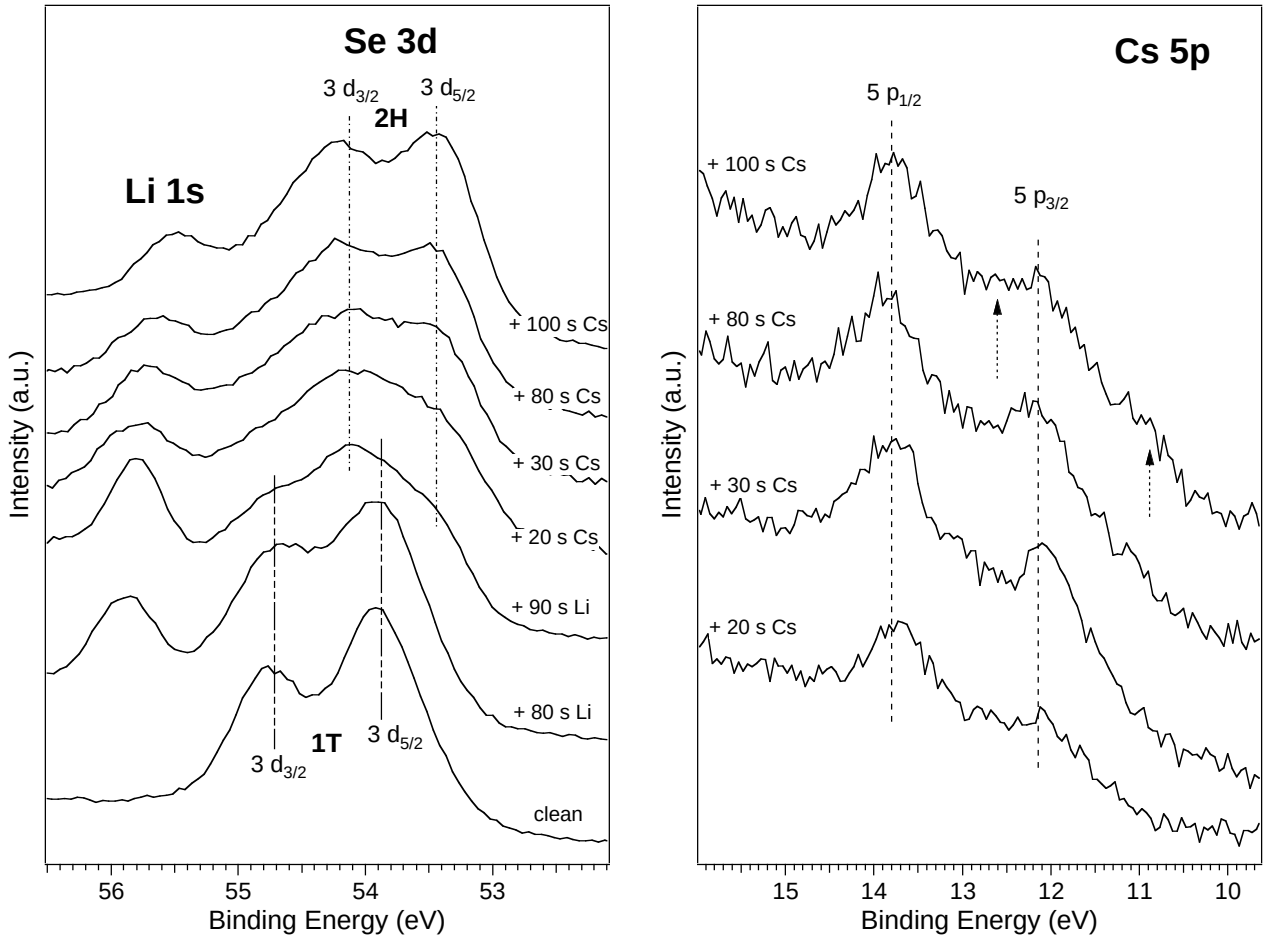

Fig. 5.30 Li and subsequent Cs deposition steps on $TaSe_2$: Li 1s together with Se 3d core-level signals are recorded with hν=80 eV (left). Cs 5p core-level emission excited with hν=21 eV (right). Arrows indicate the intercalated Cs component

The substrate intensities decrease only slightly with further Cs doses, and do not reveal new details after the Li-induced transition to the 2H phase. The decrease of the substrate intensity due to higher Cs coverage is possibly balanced by a reduced Li concentration in the surface region of $TaSe_2$. In fact if we consider the *+ 80 s Cs* dose in more detail we see a slight decrease of the Cs

signal, probably due to a reduced adsorption rate as well as to the onset of intercalation. However, the Li peak decreases more clearly, and the Se 3d becomes narrower indicating a lower degree of interaction between Se and alkali ions.

Li/Cs/TaSe₂

With the chosen Cs deposition rate on a clean substrate, the lower binding energy Cs 5p component appears soon (Fig. 5.31), from which it can be concluded that the intercalation reaction readily takes place. When Li was deposited a Cs surface component appeared, while the intercalated signal is significantly decreased. With larger Li amounts all of the observable Cs is deintercalated, and remains adsorbed on the surface. In the case of Cs deposition on a cleaved crystal the Se 3d level is much less broadened (not shown), compared to the same amounts of deposited Li or Na. Instead, the broadening occurs later with Li deposition. This confirms a much weaker interaction between Se and intercalated Cs compared to that observed when the smaller Li or Na ions are intercalated. Nevertheless, also with Cs the CDW-induced Ta 4f splitting is increased indicating that charge transfer actually still takes place with comparable relevance. It is therefore possible to distinguish qualitatively an electronic, ion-size independent effect, which leads to changes in the electronic structure and related CDWs from a purely ionic interaction. The phase transition appears to be not as complete for the same deposited Li amount as in the previous experiments, possibly due to a faster diffusion in the Cs intercalated substrate.

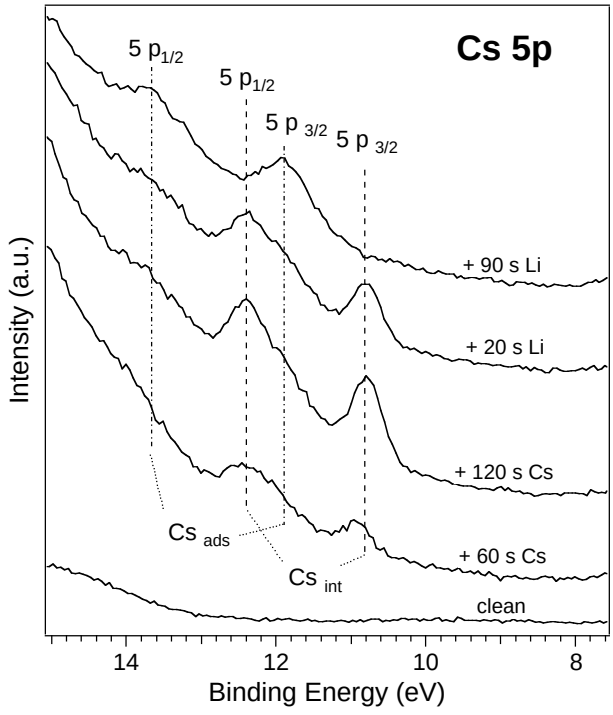

Fig. 5.31 Cs 5p core-level emission excited with hν=21 eV of the cleaved 1T-TaSe₂ crystal during Cs and subsequent Li deposition steps

Na/Cs/$TaSe_2$

On a Cs intercalated substrate Na was found to behave similarly to Li in its ability to deintercalate Cs (not shown). In this case it was however not possible to obtain a complete Cs deintercalation, confirming the slightly reduced strength of Na, compared to Li, to form the intercalated compound. No sign of 1T→2H phase transition was found during the whole experiment.

5.2.2 Halogens and Na

In order to check whether the intercalation reaction can also be reversed in UHV experiments as e.g. in electrochemical cells reactants with a high affinity to Na must be exposed to the intercalated phase. Additionally the experiment here presented will help to clarify aspects of the alkali co-deposition experiments described in §5.2.1.

Cl_2/Na/$TaSe_2$

It is possible to adsorb chlorine on intercalated layered chalcogenides kept at liquid nitrogen temperature. Cl_2 is able to induce a complete Na deintercalation from the depth accessible to SXPS experiments. The sample as shown in Fig. 5.32 was intercalated with Na at room temperature, cooled down to 100 K and exposed to 10 Langmuir of gaseous Cl_2. Although the Cl_2 coverage weakens the Na 2p peak, it is still possible to follow its position, which remains at about 31 eV up to 170 K. Rising the temperature the substrate intensities recover due to desorption of most of the Cl_2, as the decrease of the Cl_2 molecular peaks in the valence band clearly indicates. Closer to RT, a broad and much more intense peak centered at 31.5 eV clearly shows the deintercalation of Na ions. At higher temperature the ion mobility of the intercalated Na ions is increased and the diffusion to the adsorbed chlorine is possible which leads to a surface reaction. LEED pictures taken on the cleaved substrate and after deintercalation show a $\sqrt{13}\times\sqrt{13}$ structure. The main features of the substrate appear recovered as well, although all intensities are lowered, due to the formation of a NaCl overlayer. It can be concluded that the substrate maintained all its major structural and electronic properties after the intercalation-deintercalation process.

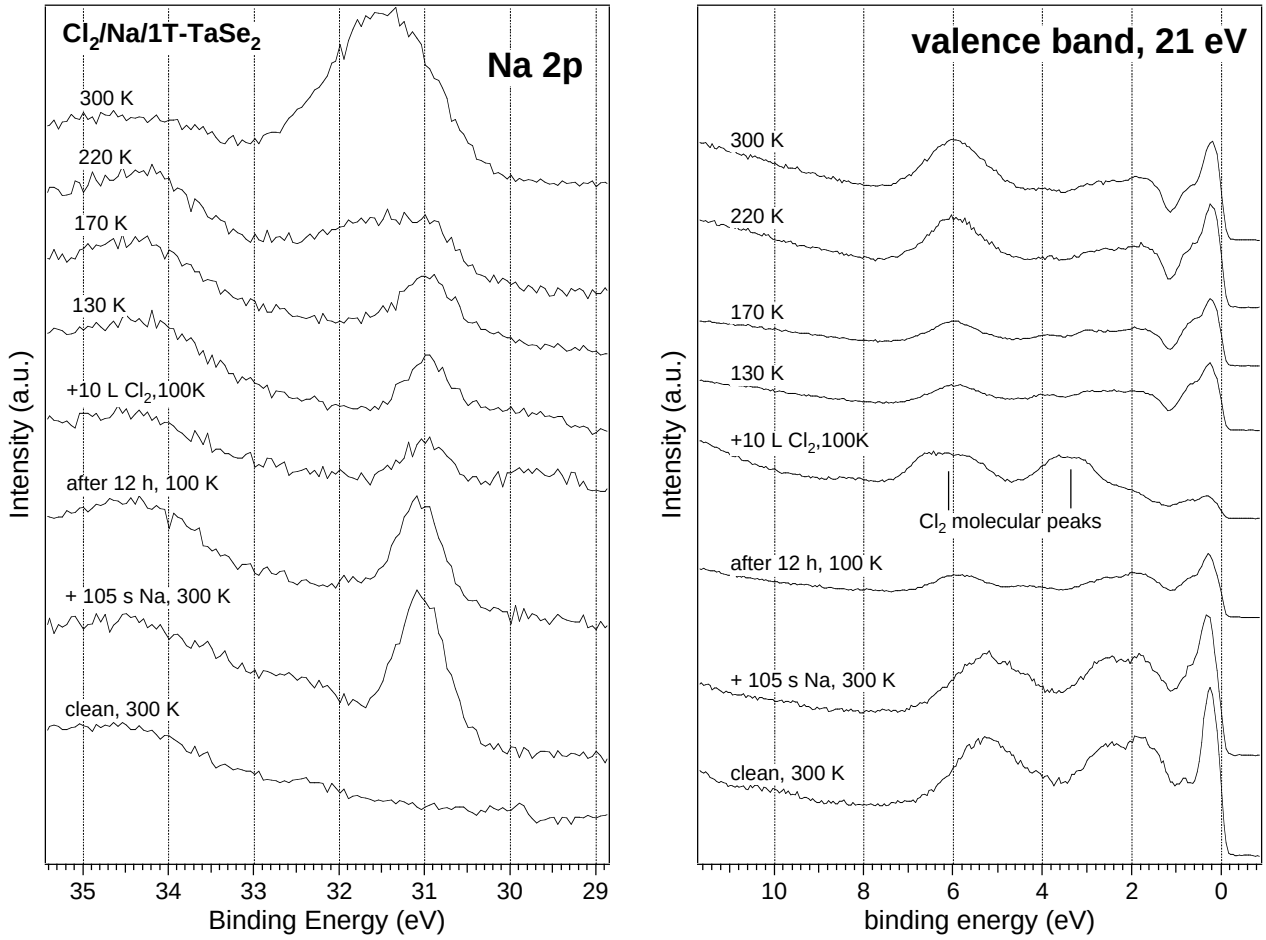

Fig. 5.32 Na 2p core-level emission excited with hν=80 eV and valence band spectra excited with hν=21 eV for the low temperature deposition of Cl_2 on Na-intercalated 1T-$TaSe_2$ (left) and of Na on Cl_2-covered 1T-$TaSe_2$ (right), and subsequent annealing to room temperature

5.2.3 Discussion: electrostatic fields and relative intercalation strengths

Direct or host-mediated interactions are responsible for rearrangements of intercalated species induced by co-deposition experiments. The four different effects found are summarized in Fig. 5.33. In addition, co-deposition experiments give further details to the understanding of the mechanism of the intercalation of alkali metals into TMDCs in UHV experiments.

It has been shown that interactions among intercalated alkali are due to essentially two factors. On one hand it is the electric field of the positive ion, which, due to the effective screening by the electrons donated to the host layers, leads to a significant repulsion only within one lattice constant [236]. On the other hand, the elastic deformations of the layered host lattice induce a repulsion perpendicular and an attraction along the vdW gap [247, 248] (see also Fig. 5.34). The effects of strains are expected to be more relevant at a longer range.

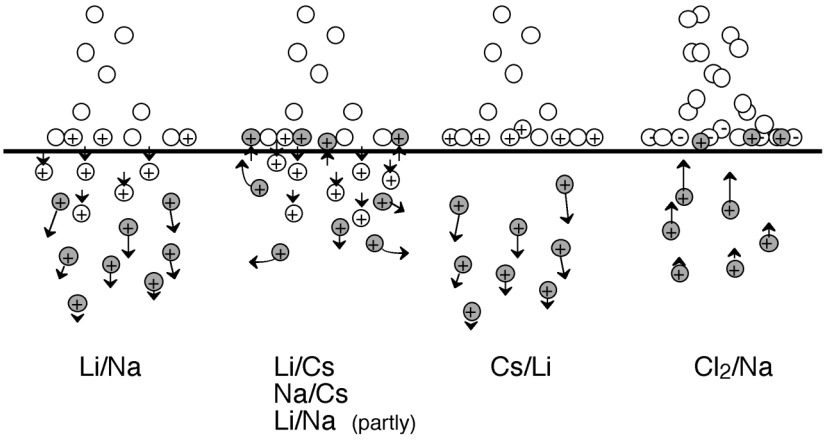

Fig. 5.33 Model summarizing the effect of co-deposition experiments. The species deposited in a first step are indicated in gray, the subsequently deposited species in white

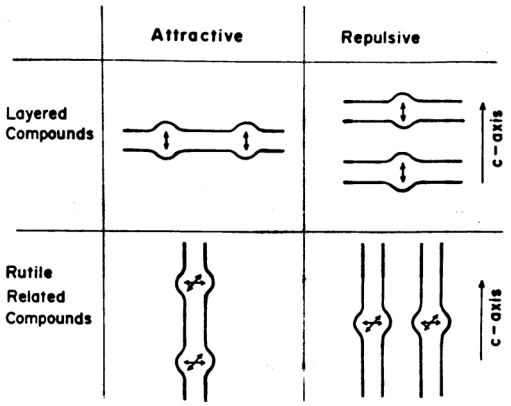

Fig. 5.34 Schematic summary of the nature of the strain-induced interaction between two intercalated atoms in layered and rutile related (channel-like) compounds. The strain is minimized when the guests are close to each other in the case both are confined in the same gap, otherwise they prefer the maximum distance. After McKinnon et al. [247]

Both Li and Na appear to intercalate fast and with a comparable free energy of formation. The observation that Li is pushed in by Na suggests that the same process happens also when only Li is deposited with progressive doses. First the alkali accumulates rapidly at the top layers, favored by the limited strain induced to the host lattice. This corresponds to the creation of a diffusion barrier for intercalation. As observed in §5.1.2 this barrier prevents an even distribution of surface intercalated alkali ions into the bulk of the substrate with time. Once the concentration of intercalated ions is so high that the mutual distances approaches the lattice constant the repulsion among the guest ions promotes the diffusion into the next empty van der Waals gap. On an energetic point of view this means that, when the guest concentration increases in a vdW gap, locally the free energy increases rapidly, and the activation barrier to diffusion becomes lower. As a result, an intercalation front forms and further deposition induces a displacement of this front into larger depths. Previously intercalated ions will be pushed further into the bulk by additionally deposited ones, and alkali intercalated in an ordered movement. If, as is the case with PES, only a few top layers can be analyzed the Na signal tends to a constant value after prolonged deposition or disappears, if instead Li is subsequently deposited.

The exchange reactions (second case in Fig. 5.33) can be explained by both the weaker ion-host layer electrostatic attractive interaction and increased host lattice strain for a larger ion.

Possibly the strain is also responsible for the absence of mixed intercalated phases, which include alkali of different sizes. The free energy of a mixed intercalation phase is higher than compared to the situation for the larger alkali adsorbed on the surface. Therefore its deintercalation is favored compared to its deeper penetration into the bulk.

The fact, that Li is pushed inside by adsorbed Cs suggests the existence of a repulsive electrostatic interaction between intercalates even across the slabs. On a macroscopic point of view we should not expect any electrical field inside a metallic conductor. However, on an atomic scale this should not hold any more, and it is likely that the positive charge of intercalated ions cannot be compensated or screened across the van der Waals gap as a consequence of the hindered mobility of charge carriers along the **c**-direction (normal to the van der Waals planes). The existence of this interaction, in its attractive form seems to be also confirmed by the fast Na deintercalation induced by adsorbed chlorine (fourth case in Fig. 5.33).

The two driving forces for the intercalation can be compared using these results combined with those obtained by Starnberg (ref. [222]). The tendency to form intercalation compounds is increased in the sequence Li≥Na>K>Cs. If the work function difference between alkali and substrate would be the dominant effect, the sequence should be Cs>K>Na>Li, as e.g. it may be deduced from the work function (1.95, 2.29, 2.75 and 2.93 eV for polycrystalline alkali metals [216, 249]). The experimental results indicate that this sequence is not followed. Therefore the bonding interaction of the intercalated ions inside the lattice, which is dependent on the ion size, must also be considered as an important part of the free energy gain due to intercalation. On the other hand the reduction of the van der Waals inter-layer interaction, leads to a destabilization of the intercalation compound that also favors alkali ions of smaller size.

5.3 Deposition on thin films

The fast diffusion of deposited alkali into the bulk limits the intercalation concentration to low x values by UHV deposition experiments. The minimal crystal thickness to obtain after cleaving is about several μm. The used alkali dispensers do not have the capacity to intercalate a bulk crystal up to x=1. Moreover, for longer evaporation times or rates metallic alkali may accumulate on the surface, and problems with surface contamination would arise, as the Na/TiS_2 experiment has clearly demonstrated. To obtain higher x it has been attempted in the present work to use the host material in the form of a thin film on a non-intercalating substrate. The thin film should exhibit electronic properties similar to a single crystal, but with a thickness well below 1 μm. In this way if a low-concentration intercalation front builds up, it would readily reach the end of the sample, and further deposited alkali would be forced into the same limited space. In order to obtain high quality PES signals the surface has to be adsorbate-free. This is achieved at best if the

thin film is prepared *in situ* in a chamber directly connected to the UHV analysis system excluding any possibility of air contamination. The preparation and characterization of thin films have been described in the previous chapter, in this section the effects of intercalation will be reported.

The electronic structure of the system Na/TiS_2 is particularly interesting to be investigated at high *x*. As mentioned in §2.2.1 in Li/TiS_2 no phase changes have been found along the whole *x* range, whereas in Na-intercalated TiS_2 a shift of the slabs occurs in the region $0.4<x<0.7$, for which Na has a trigonal prismatic coordination [34]. The Na/TiS_2 phase diagram has accurately been studied by comparing X-ray diffraction and nuclear magnetic resonance by Molinie *et al.* [225], who found that structural changes are correlated with changes in the electronic structure. In particular with the transition at $x\approx0.7$ the TiS_2 slabs become thinner and the $DOS(E_F)$ increases suddenly.

The Na emission signals, which were typically obtained after deposition onto TiS_2 thin films, are shown in Fig. 5.35. They always show a bulk component together with a surface component with nearly constant ratios, which were found to be sample-dependent. It may be argued that the highly textured samples may exhibit areas, which were less intercalated, e.g. Ti-rich phases. The presence of adsorbed Na may also be stabilized by the roughness itself[‡]. In spite of this relatively high surface Na amount the O content at the surface could be kept low until a new source was used. With the new source, due to the higher evaporation rate, Na readily covered the sample. Some oxygen was found after this last deposition step. As for Na/TiS_2 the Na 1s integrated area in this case overestimates the amount of intercalated Na. The Na KLL signal must be then evaluated for intercalated Na. This procedure has been used here, too.

[‡] Li intercalation in carbons with amounts higher than the believed theoretical limit of LiC_6 has been explained with the absorption in microcavities such as pores and voids of the electrode [250]. In a so-called “house of cards model” [251, 252] it is postulated that in extremely disordered carbons Li can adsorb on both sides of single graphene sheets.

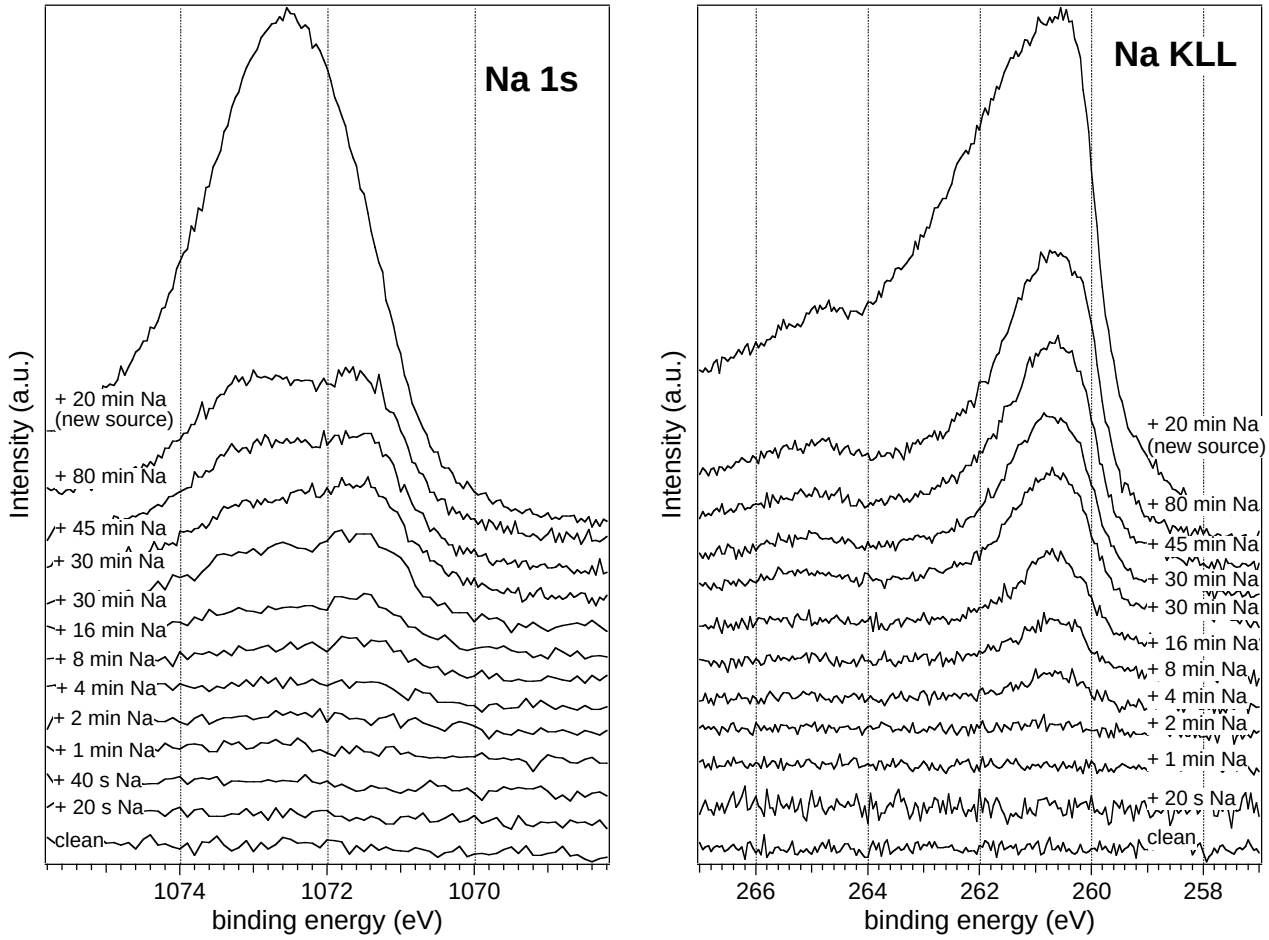

Fig. 5.35 Comparison between the Na 1s core-level and Na KLL Auger emission of a TiS_2 thin film at increasing Na deposition times

If compared with the Na deposition on single crystals, the Na/Ti ratio shows a much more linear increase. However with formation of a surface species the intercalation yield decreases, and the value calculated from the Na KLL spectra indicates a lower slope, if compared to the points calculated from the Na 1s spectra. The experiment was affected by the formation of the surface species, but there is no evident sign of a maximum Na concentration.

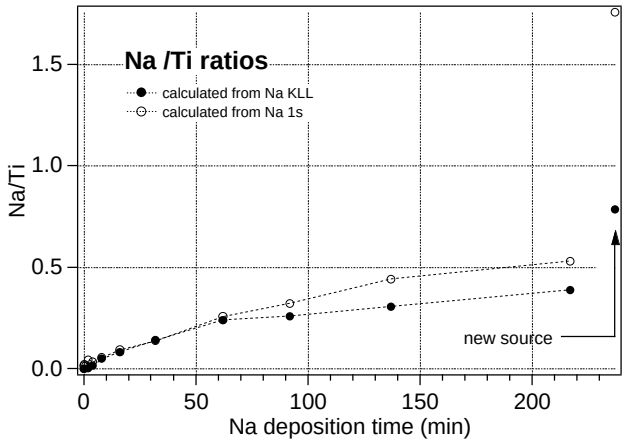

Fig. 5.36 Na/Ti ratios as calculated from the integrated intensity of the total Na 1s peak and of the intercalated component deduced from Na KLL spectra

Due to the different crystal orientation a direct comparison of He I and II valence band spectra with single crystals is not possible. However the main peaks can be recognized and have been marked with the usual notation. The peak labeled as “E” was not identified in single crystals. According to some partial density of states calculations it corresponds to the main Ti 3d contribution in the valence band [40, 46, 163]. The interpretation is confirmed by the corresponding He II spectra, where peak E is even more evident. The relative Ti 3d/S p cross sections are 6.7 for He II and 1.2 for He I [90, 136]. According to this assignment it can be seen from the decrease of peak E that the compound becomes less hybridized upon intercalation in agreement with XANES measurements on Li/TiS_2 by Wu *et al.* [83]. A direct consequence of the lower hybridization is a higher ionicity of the Ti-S bond, as also confirmed by theoretical calculations [82, 163]. Shifts of peaks C and D can be clearly noticed also in this case as well as the opening of the S 3p/Ti 3d gap. A superposition of peak A, similar to that made in Fig. 5.3, is not possible in this case, because the shape is considerably altered by the higher secondary emission of this sample.

The sudden increase of $DOS(E_F)$ was expected for $x \approx 0.7$ based on NMR evidences [225] and theoretical calculations [163]. A possible reason for this disagreement is the effect of the covering layer of adsorbed Na, which should sensibly weaken the valence band signal. Since the higher electronic kinetic energies (lower BE) correspond to shorter free mean paths in the sample (see the universal curve for values typical of the He I excitation, 5-25 eV, Fig. 3.2) the effect of this coverage is more marked at the Fermi level than for the other features in the valence band. Thus, it is not possible from this experiment to confirm such effect.

The core-level spectra show signals and developments close to those observed for the single crystal systems $Na/TiSe_2$ and Na/TaS_2. Therefore with respect to intercalation the thin film has a behavior similar to single crystals. The Ti 2p spectrum obtained with the maximum Na amount clearly shows a second component at the low BE side (455 eV for the Ti $2p_{3/2}$). The corresponding S 2p spectrum also features a new component. The formation of a new chemical environment, induced by the presence of Na in TiS_2, seems quite evident from the parallel appearance of these new components. The nature of this effect will be discussed in more detail below (§5.4.3).

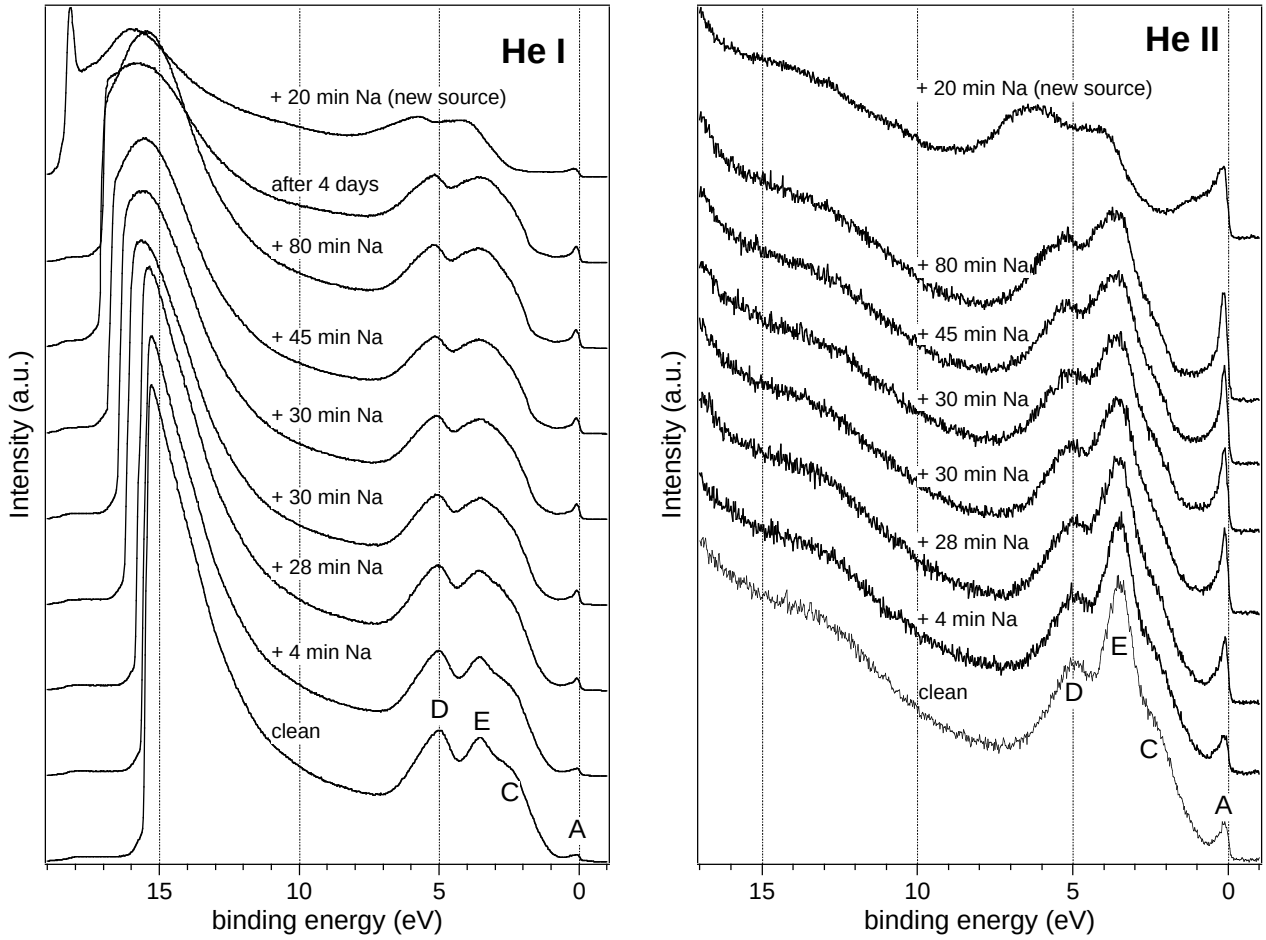

Fig. 5.37 Valence band spectra measured with an excitation energy of 21.2 eV (He I) and 40.8 (He II) on a TiS_2 thin film after deposition steps of increasing Na amounts or after resting times

As reported in Fig. 5.37, practically no variation in the He I spectra occurred after many days. This indicates that a thin film on a metallic foil can be considered as homogeneously intercalated after deposition. Further evidence is given by the experiment reported in Fig. 5.39. Na was evaporated with a fresh Na dispenser in one step for 4 minutes, which corresponded to a value of *x* of about 1, and afterwards the sample was heated at 200°C for 20 minutes. The annealing caused only a slight change in the surface structure of the intercalated film in contrast to the effects observed with single crystals.

The very low secondary emission background of the clean sample may indicate a highly ordered layer orientation perpendicular to the substrate. Na intercalation introduces a disorder, and a dramatic increase of the secondary emission. Heating induces a further increase, while a surface dipole, which formed with deposition, was at least partially removed. This indicates, as is expected, that for Na atoms intercalation is energetically favored with respect to the surface interaction. The shoulder formed at 8.2 eV (Fig. 5.39) and then removed may be associated with a chemical interaction of Na atoms with sulfur dangling bonds at the platelets' edges. This interpretation is supported by He II spectra, where no feature is visible at 8.2 eV. He II spectra are even more

surface sensitive and no change at all could be noticed. The S 2p core level, however, is less surface sensitive, and reveals a moderate shift backward to lower BE after heating. Also the extent of the higher BE component decreased slightly by heating. This experiment suggests that even before annealing no Na accumulation occurs close to the surface and its distribution can be considered already nearly equal along the film's depth. As a consequence in the case of a thin film substrate the intercalated alkali concentration is nearly proportional to the deposited amount.

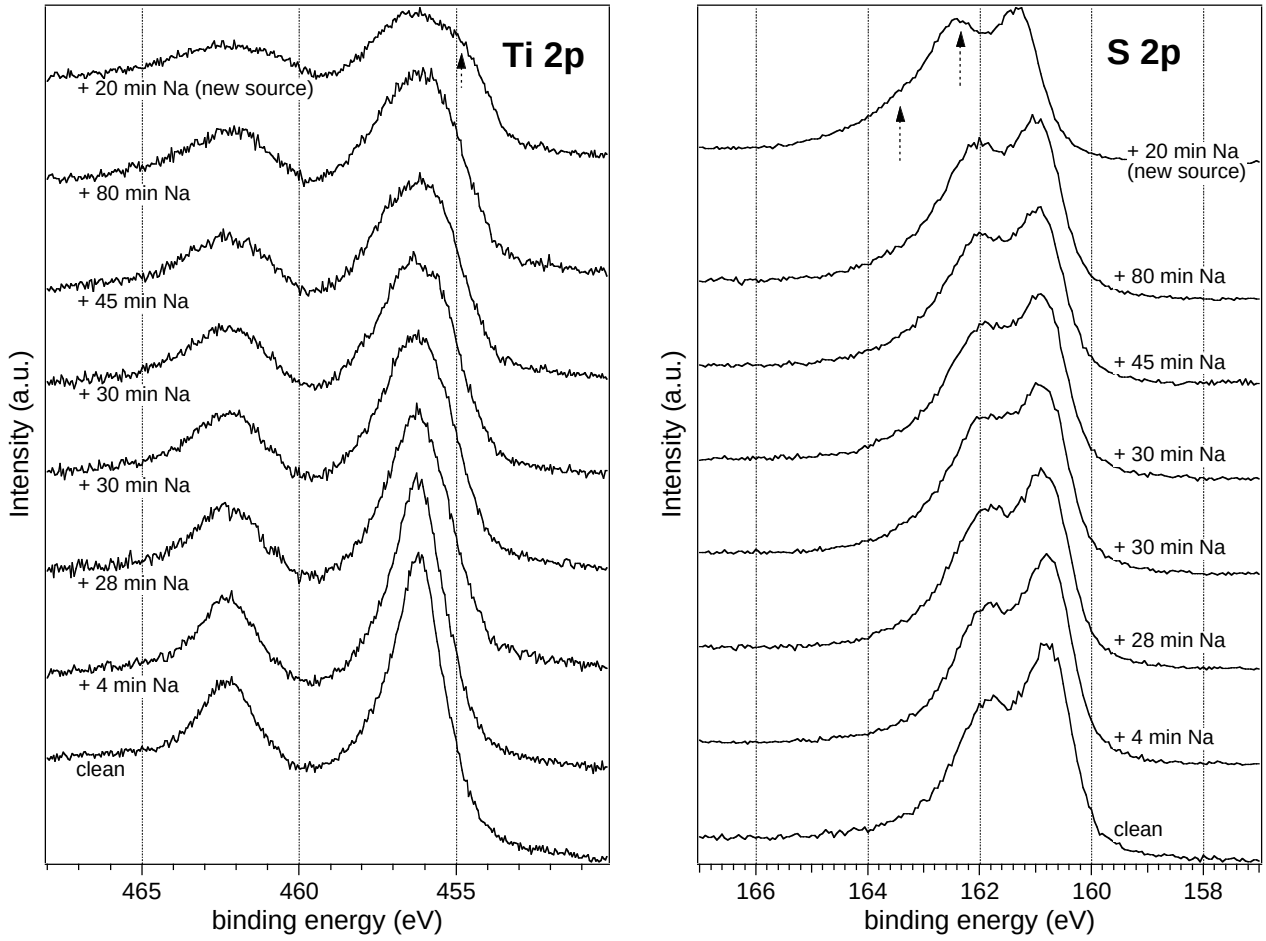

Fig. 5.38 Ti 2p and S 2p core level spectra on TiS_2 thin film after deposition steps of increasing Na amounts. Arrows mark the new components developed after the last Na deposition step

As already observed, the dependence of the Na/Ti ratio calculated from the Na 1s and Ti 2p peaks vs. deposition time is nearly linear (see also Fig. 5.41). This indicates that the sticking coefficient of Na on the substrate is constant, and presumably close to 1. It demonstrates that with thin films it is possible to study the intercalation reaction in a wide stoichiometry *x* range. The slopes changed strongly from sample to sample. This may be due to different substrate thickness and to different deposition rates, which depend on the operation time of the Na dispensers.

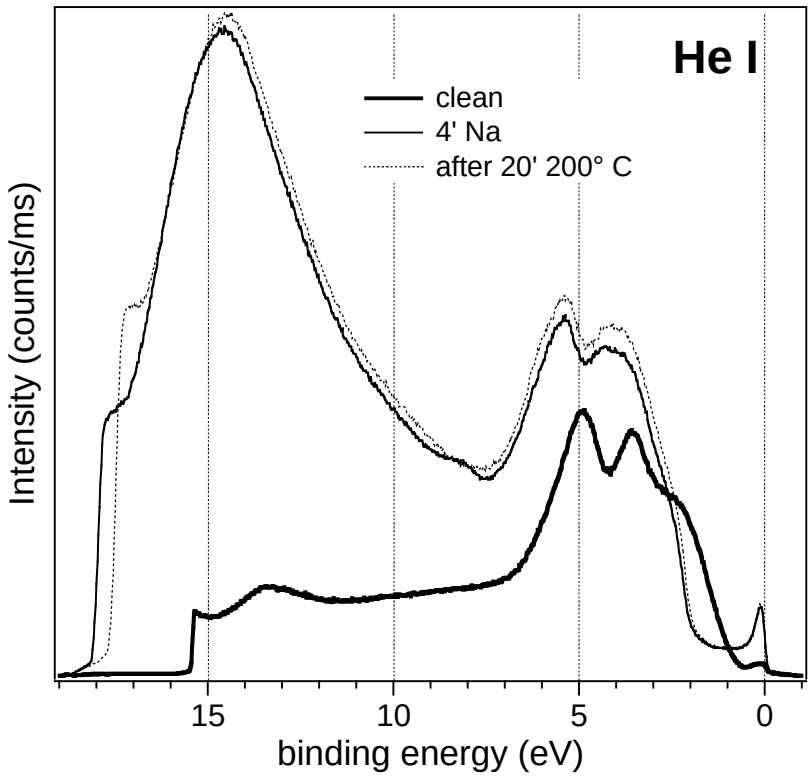

Fig. 5.39 Valence band spectra of TiS_2 thin film excited with He I radiation for a pristine, and for a Na intercalated thin film, before and after heating 20 minutes at 200°C

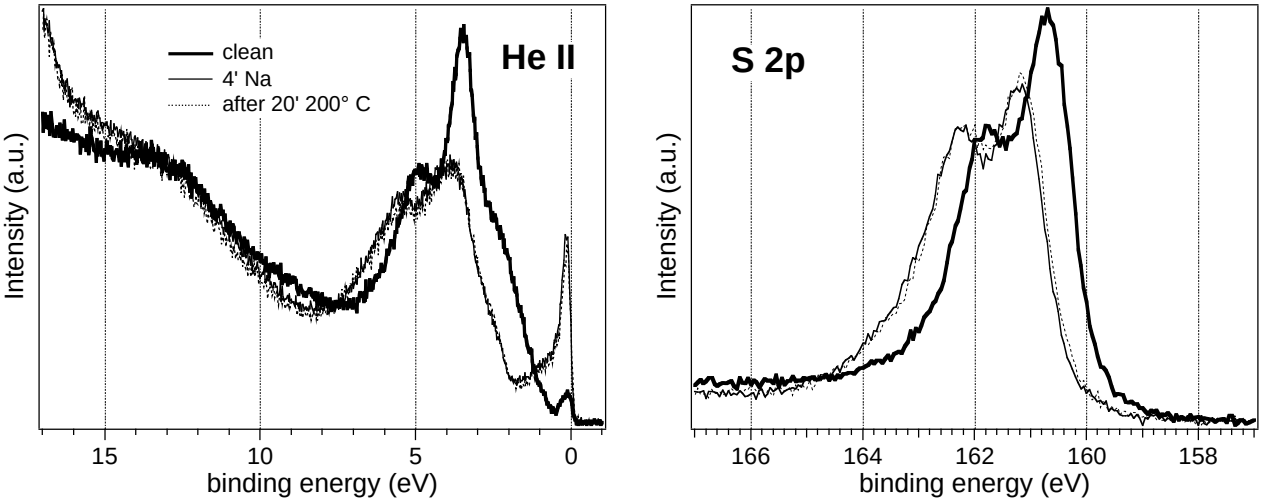

Fig. 5.40 Comparison of the effects of Na deposition and heating between surface (He II) and bulk (S 2p XPS)

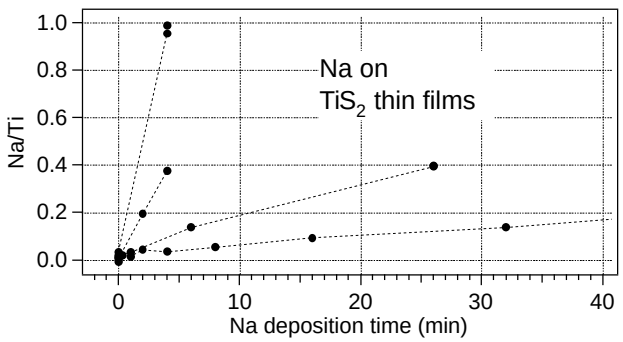

Fig. 5.41 Dependence of the Na concentration on the Na deposition time for different TiS_2 thin films

5.4 In-situ electrochemical intercalation

The development of thin film synthesis for deposition experiments opened the way to a more elegant experiment. If instead of depositing the thin film on a metal foil a solid electrolyte is used as a substrate, it is then possible to prepare a complete electrochemical cell in vacuum, where one electrode can electrochemically intercalate exactly in the same way as if it is part of an operating battery system. At the same time this electrode can be investigated by photoelectron spectroscopy just as in the previous experiments. This may in principle allow to characterize each state of intercalation with both its electronic structure and its electrochemical parameters, first of all the voltage.

5.4.1 The electrolyte

Na-β Al_2O_3 is a well-known solid electrolyte of high Na^+ mobility, discovered in 1967 by Weber and Kummer [253]. Its most important applications are in ion-selective filtration and purification, electrochemical sensors, batteries (in particular sodium-sulfur [254, 255]) and fuel cells, as well as catalysis. It is also used in electrochemical promotion (EP) of catalytic reactions, an effect discovered more than a decade ago by Vayenas and co-workers [256]. This technique is based on electrochemical pumping of ions from a solid electrolyte to the surface of a porous, catalytically active metal film in contact. Na formed at the metal electrode/solid electrolyte/gas three-phase boundary alters the catalyst's surface electronic properties, first of all its work function. By controlling the catalyst potential it is thus possible to tune its activity. Lambert and co-workers have shown that EP samples can be studied by surface science techniques [257-262]. Based on these results this material has been chosen in the present work as electrolyte for the TiS_2 thin film cathode.

Na-β Al_2O_3 is the traditional name of a sodium hexaluminate of formula $Na_2O{\cdot}11Al_2O_3$. The hexagonal crystal structure consists of an arrangement of NaO layers and $Al_{11}O_{16}$ spinel blocks. An excess Na is always present, balanced by an excess of oxygen. The fast ionic conduction arises from the excess and disorder of sodium ions. In order to increase the conductivity and improve the stability typically some Al^{3+} ions in the spinel blocks are replaced by divalent cations [254]. The β'' alumina is a related metastable phase with rhombohedral symmetry and enhanced conductivity.

5.4.2 Sample preparation

Commercial plates of Mg-stabilized Na-β''Al_2O_3 (Ionotec [263]) 1 mm thick were cut to a size of 12 x 16 mm and used as substrate. The counter-electrode consisted of a graphite layer, obtained by casting of commercial colloidal graphite (Aquadag, from Achelson AG) onto the

alumina substrate. After drying a compact film of 2-5 µm thickness was obtained, as deduced from SEM (Fig. 5.42) and profilometer measurements.

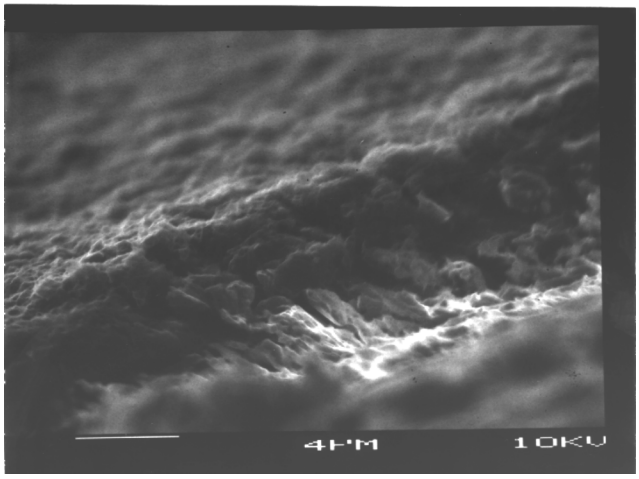

Fig. 5.42 Cross-section SEM micrograph of a C layer deposited onto Na-β''Al_2O_3 from colloidal graphite

Na can be inserted into graphite to form high-stage intercalation compounds NaC_{8n}, [264]. However, using different disordered carbons it has been shown that faradic insertion processes with larger amounts are also possible depending on the disorder and on the grain size [265, 266], and battery performances similar to those with metallic Li can be achieved [267]. A cell graphite/Na-β''Al_2O_3/Na was prepared by placing the plate on a heater at 180°C in an Ar filled glove box, and melting directly a Na drop on the clean side. When Na wetted the solid electrolyte an open circuit potential (OCP) of typically 2.7 V could be measured. This possibly corresponds to the equilibrium reaction:

$$C_8 + Na^+ + e \rightarrow NaC_8 \qquad \textit{(Eq. 5.1).}$$

As the NaC_8 amount is extremely small the equilibrium potential could be easily altered with a very small charge (see Fig. 5.43). Therefore the graphite electrode is highly polarizable and cannot be considered as a reference, at least in the 2-electrode configuration.

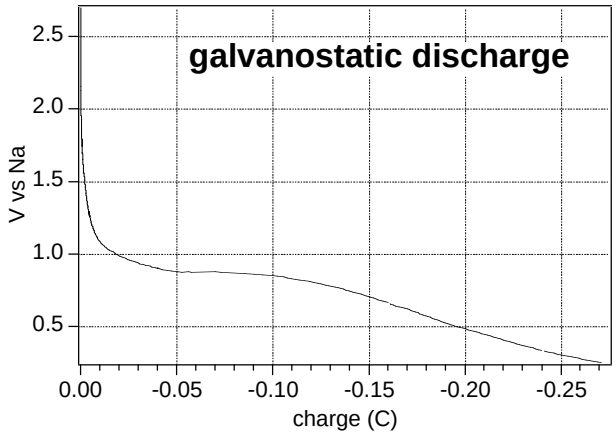

Fig. 5.43 First galvanostatic discharge curve for a graphite/Na-β''Al_2O_3/Na cell at a constant current of –2 µA

By keeping the cell at low voltage the graphite could be loaded with Na shifting to a potential characteristic of its intercalation stage. If a rocking-chair cell is assembled with an

electrode much thicker than the other, the potential of the thick electrode may be considered constant during its operation, and the cell voltage would vary only due the potential of the thinner electrode. The thicker electrode would act as a reference for the thinner. Using the thick (>2μm vs. <100 nm of TiS_2) intercalated graphite as counter electrode the cell voltage could be easily related to the TiS_2 potential changes. However, if after equilibration the sample was shortly exposed to atmospheric moisture the OCP was found to increase up to values larger than 1.6 V. In analogy with the Cl_2/Na/TMDC system it can be easily imagined that a large part of the inserted Na deintercalates to reduce H_2O with formation of NaOH. Therefore during the transfer from the Ar-glove box to the vacuum system the graphite electrode must be protected from air. Lacking of a transfer box, which could be connected to the insertion lock, it was attempted to use a coating on the graphite layer. But it was not possible to find a suitable sealing able to both protect the sample and not to interfere with the following operations in UHV.

Being unable to pin the graphite potential at a nearly constant value by intercalated Na, it was interesting to investigate the anodic reaction at this electrode. The symmetric graphite/Na-β''Al_2O_3/graphite cell was prepared and transferred to an UHV chamber containing a mass spectrometer and connected to a potentiostat. By imposing a positive constant current to the cell Na^+ migrates to the counter electrode. The counter electrode is intercalated and its electrochemical potential decreases just as discussed for the symmetric graphite/Na-β''Al_2O_3/Na cell. The potential of the opposing working electrode increases as long as no occupied electronic states are available, i.e. species can be oxidized. As expected from the high stability of both graphite and Al_2O_3 the voltage increases very rapidly, until a plateau of +5.4 V is established (Fig. 5.44). A stable voltage at a constant current is typical for reactions involving a species that is readily available at the electrode. In a 2-electrode cell this must be true for both anodic and cathodic reactions. By inverting the current the plateau at –5.4 V, corresponding to the reverse cell polarization, is readily established. The reversible charge is very small indicating a poorly reversible processes. The reversibility of one of the two reactions would lead to an intermediate plateau. The opposite voltage indicates that exactly the same reactions take place at reverted electrodes. At currents of the order of 100 μA it was possible to observe an increase of the chamber pressure of some 10^{-10} mbar, with a prompt decrease if the current was inverted. The mass spectrometer detected only a mass of 32 amu, which was following the total pressure variations. This value is characteristic of O_2, and all observations indicate that at the plateau voltage the electrolyte is decomposed according to the half-reaction:

$$Na_2O \rightarrow 2Na^+ + \tfrac{1}{2}O_2 + 2e \qquad \textit{(Eq. 5.2).}$$

Oxygen development has also been noticed at Na-β''alumina at large anodic potential using Cu and Au electrodes by Lambert and co-workers [261].

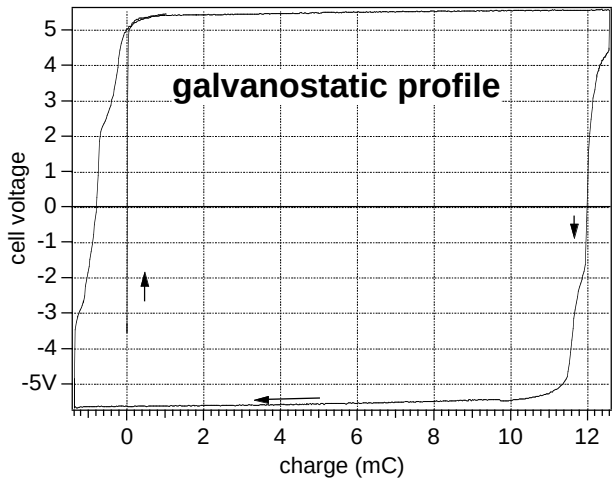

Fig. 5.44 Galvanostatic voltage profile at a 1 μA rate for the symmetric graphite/Na-β''Al_2O_3/ graphite cell in UHV

In order to limit to some extents the electrolyte decomposition during anodic polarizations, the graphite intercalation was executed as described above, despite the transfer in air. Residual intercalated Na should limit the electrolyte decomposition and O_2 development. The Al_2O_3 plate was then mounted onto the Leybold carrier with the graphite film on the bottom and the clean side on top, and inserted into the UHV preparation and analysis system.

A TiS_2 film was deposited as described in Chap. 4. In order to prevent any electric contact with the backside, a mask with an opening of 1 cm^2 covered the substrate surface. The electric contact to the cathode was obtained after deposition by mechanically flipping a Mo wire onto the TiS_2 surface. In this way any formation of short circuits with the back side could be excluded.

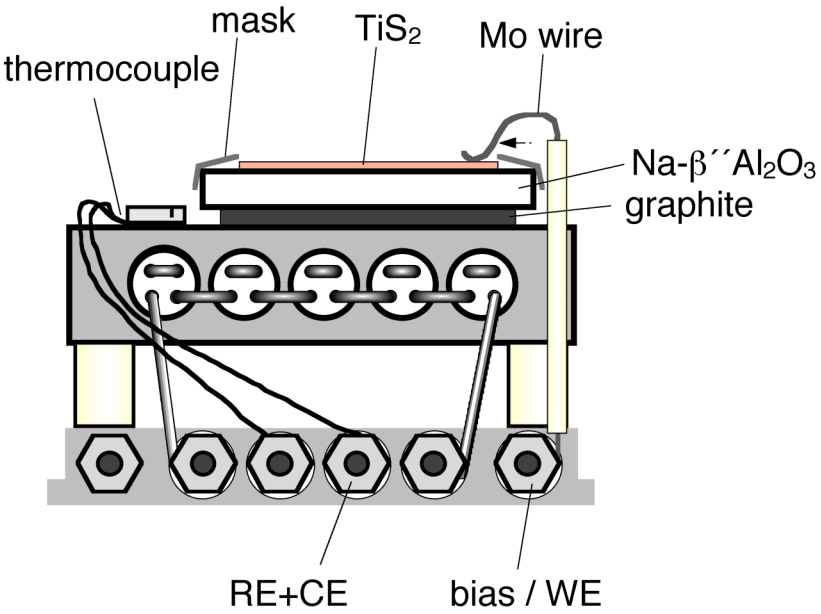

Fig. 5.45 Scheme of the TiS_2/Na-β''Al_2O_3/graphite electrochemical cell mounted on the Leybold carrier

Electrochemical data were collected with a EG&G PAR 362 potentiostat, either in controlled potential or controlled current mode, connected in a 2-electrode configuration. The

working electrode was connected to the TiS_2 film, and counter and reference electrode to the graphite layer. Since with this potentiostat the impedance between working electrode and ground is 50 kΩ, the sample Fermi level was at a potential iR higher than ground. Spectra measured not at zero current (i.e. in OCV) have been shifted in energy in order to keep this effect into account.

5.4.3 Results

The TiS_2 film was contacted after preparation. Spectra measured before and after contacting differ not only because of the shift induced by charging. Also the Na content increased sensibly (Fig. 5.46). The Mo wire was turned with a transfer rod in contact to ground, which induced a short circuit during this operation. The fact that a discharge with Na intercalation results proves that the graphite had a lower potential, because residual intercalated Na was actually still present in this layer. Indeed, an open circuit voltage of about +500 mV could be measured after the contact was established. But evidently the amount of Na was too small to induce a complete intercalation of the TiS_2 thin film.

When the voltage between the front TiS_2 and the back graphite electrode was kept at +2.4 V the thin film cathodes showed PS spectra identical to samples prepared on a metallic Ti foil. The only exception were Na and Cl impurities, found in a ratio of 1:1. The Na KLL Auger peak measured at this stage is located at about 264 eV (Fig. 5.46), which indicates an oxidized form of Na. It is likely that NaCl is formed during the film synthesis by a reaction involving either $TiCl_4$ or chlorine and the beta alumina's sodium. The initial Na/Ti ratio was found to be about 0.15. Due to this offset the *x* values will be estimated from the intercalated Na KLL component.

When the applied voltage is decreased the Na amount in the sample is found to increase, as clearly shown by both Na 1s and Na KLL signals (Fig. 5.46). The latter also indicates that the additional Na has a much lower binding energy than that of the NaCl contamination initially present in the sample. The Na/Ti intensity ratio *x* is directly correlated with the charge calculated as time integration of the current measured between working and counter electrode (Fig. 5.47), indicating that no significant side reaction took place during intercalation. No significant time effect on the PES intensities was observed without passing any current between working and counter electrode. This confirms that the thin film was homogeneously intercalated with the Na from the Na-containing Na-β''Al_2O_3.

The charge/*x* ratio may be used to estimate the film thickness, assuming a homogeneous TiS_2 layer. Given the charge *Q* required to intercalate 1 equivalent Na, and the sample area S, the thickness *z* can be calculated as:

$$z = \frac{Q}{F}\frac{FW_{TiS_2}}{S \cdot \rho_{TiS_2}} \qquad \textit{(Eq. 5.3)},$$

where F is the Faraday constant, FW and ρ respectively the formula weight and the density of TiS_2. A value of 18 nm is obtained, in reasonable agreement with the sample thickness and the roughness determined by AFM (Chapter 4).

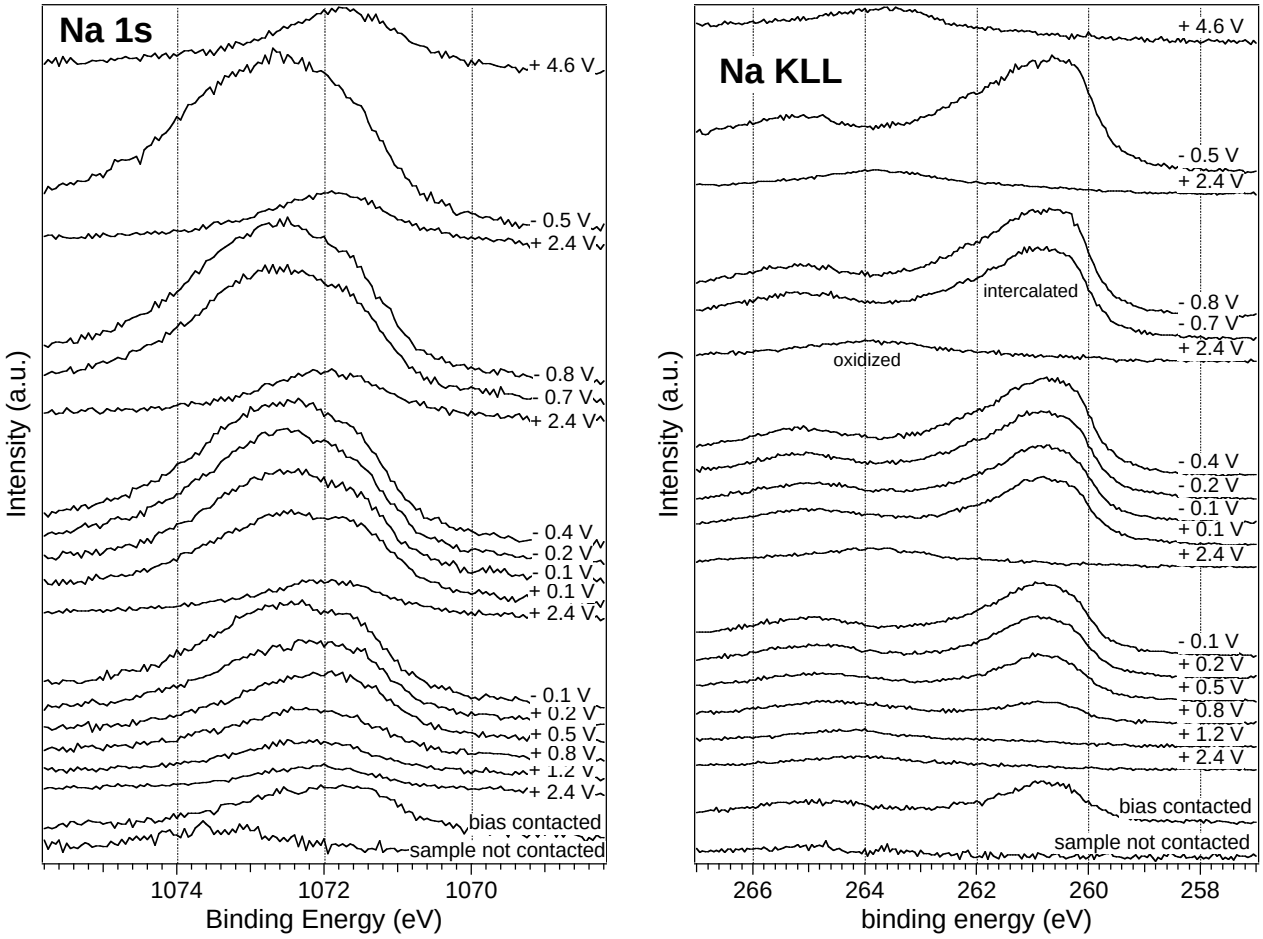

Fig. 5.46 Na 1s and KLL signals excited with Mg Kα radiation recorded at different intercalation (discharge) stages followed by deintercalation (recharge)

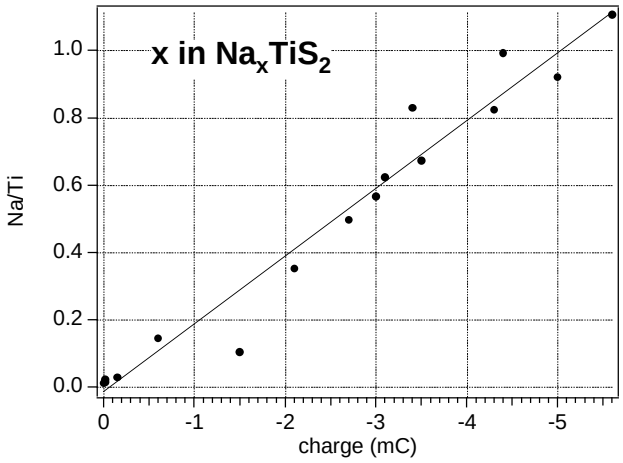

Fig. 5.47 Correlation between Na concentration x, calculated from Na KLL and Ti 2p intensities, and electric charge calculated from the cell current

It was possible to intercalate and deintercalate the TiS_2 electrode with good reversibility for several times by just switching the potential from a value of +2.4 V to -4 V. As with deposition onto thin films the Na signals seem to exhibit two components growing with approximately constant ratio (see also Fig. 5.46). After many intercalation-deintercalation cycles a slight increase of the irreversible Na amount is shown by the increase of the oxidized form in the Na KLL spectra. The nature of this species is not clear. The corresponding Cl 2p and O 1s peaks remain constant. For the deintercalated electrode the work function keeps the constant value of 5.9 eV, so that the formation of Na adatoms at the surface can be ruled out. Most likely a reaction with S from the substrate occurs with formation of a Na sulfide. However, the S 2p spectra at +2.4 V polarizations do not show any new feature.

But at very low potentials, a sharp Na KLL peak located at 259.0 eV shows the formation of metallic Na segregation phases (Fig. 5.48). For this voltage a work function of 3.6 eV was measured, which is substantially higher than 2.75 eV corresponding to polycrystalline Na [216], and a step in the secondary electron onset at higher BE (corresponding to a lower work function) could not be recognized. This suggests that the Na metallic-like phases are either not present on the surface or form clusters. The valence band spectrum also reveals the metallicity, with a high DOS up to E_F. To note is the intense peak at the same position of peak C. Its intensity and narrow width indicate a high localization of the electrons and suggests the formation of a S adsorbate layer on the surface of the sample. The attribution of peak C to O 2p derived from the adsorption of oxygen-containing compounds is unlikely, because this requires that the O_2 developed during this experiment (partial pressure $<10^{-10}$ mbar) adsorb on the sample at RT. The literature reports for Li_2O a band centered at 5.5 eV. This agrees also with spectra reported in Fig. 5.1, where, however, the large water amount was collected during deposition, when the high temperature of the dispenser may have desorbed it from the chamber walls.

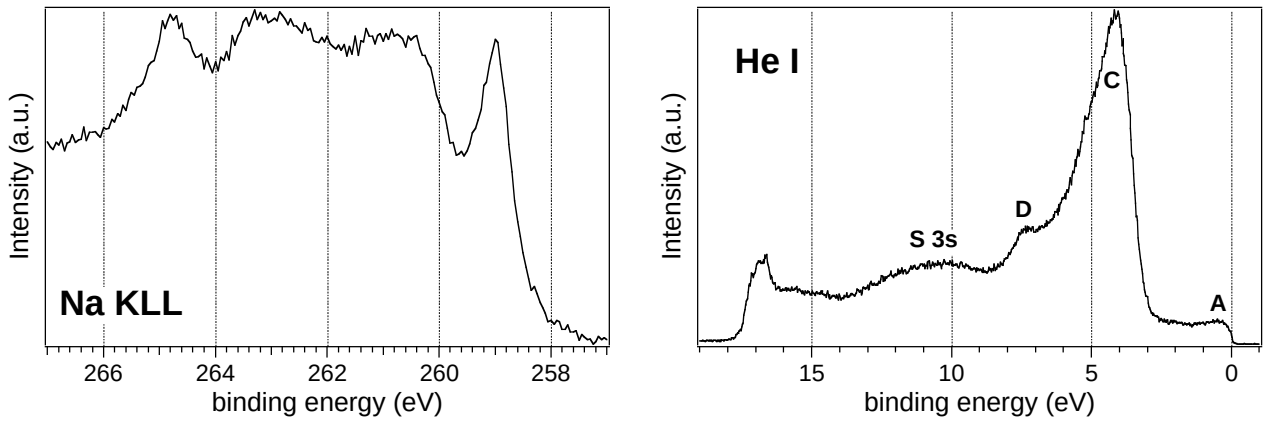

Fig. 5.48 Na 1s and He I spectra for a TiS_2 cathode with cell polarized at –6 V

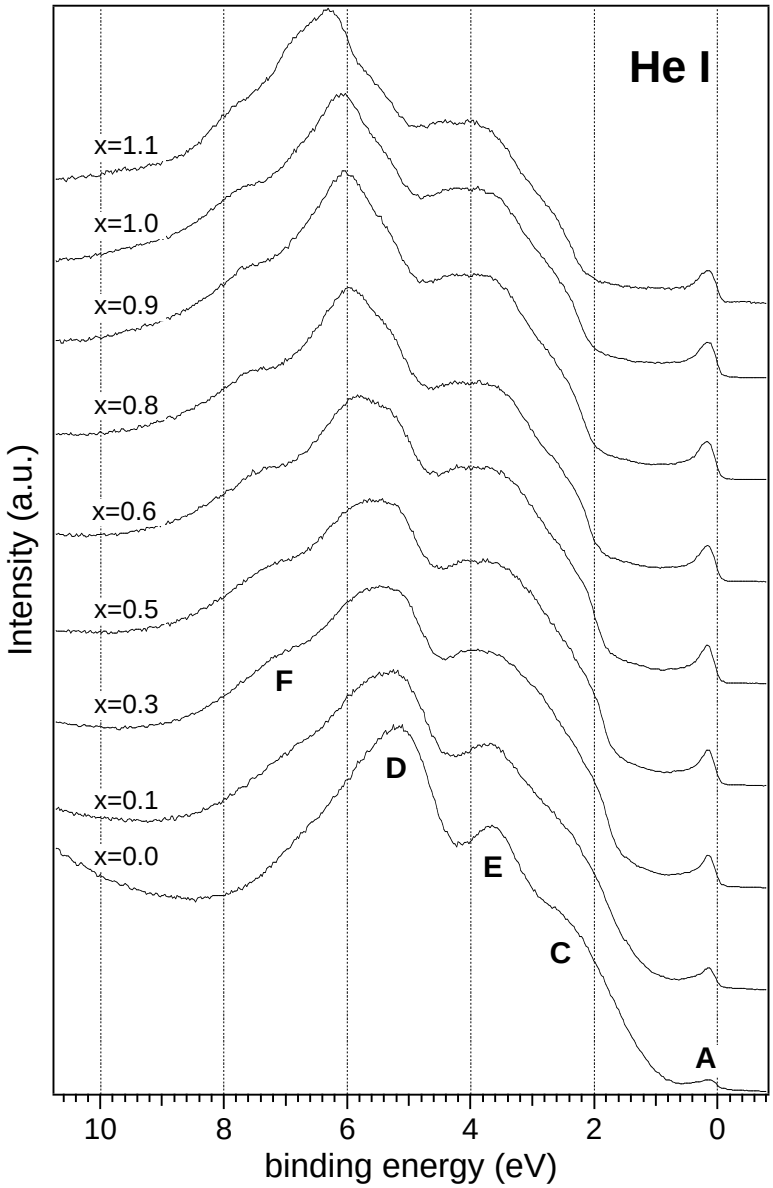

Fig. 5.49 Valence band spectra measured with an excitation energy of 21.2 eV (He I) on a TiS_2 thin film electrochemically intercalated. Spectra are given with increased Na concentration. Peaks are marked with the notation used in the previous sections of this chapter

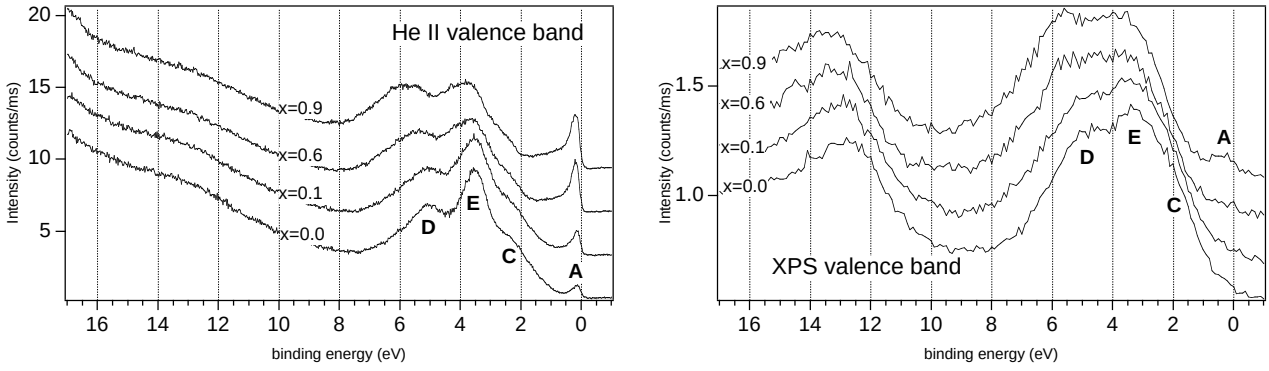

Fig. 5.50 Comparison between valence band spectra measured with excitation energy of 40.8 eV (He II) and 1253.6 (Mg Kα) for a TiS_2 thin film electrochemically intercalated. Spectra are given with increased Na concentration

As the Na signals also the effects in the valence band (Fig. 5.49) run parallel to those obtained with deposition on thin films. The S 3p/Ti 3d band gap continues to increase with *x* along

the whole composition range. The S $3p_z$ states follow the same shifts, and the Ti 3d admixture continues to vanish. Valence bands recorded with X-ray excitation show basically the same effect but revealed an apparently smaller gap than those measured with He I photons. This can be related to the reduced resolution.

A peak indicated as F is present in the top He I spectra of Fig. 5.49. It is not reversible, as it developed during polarizations at low voltage and remained at high voltage (Fig. 5.51). Since no new components developed in the spectra of the core levels at high voltage the chemical environment of both Ti and S should not change. A different S hybridization seems to be the cause of these states, which are not revealed by He II and XP valence band spectra. Possibly the intercalation of large Na amounts induces disorders in the slab stacking that cannot be totally recovered upon deintercalation.

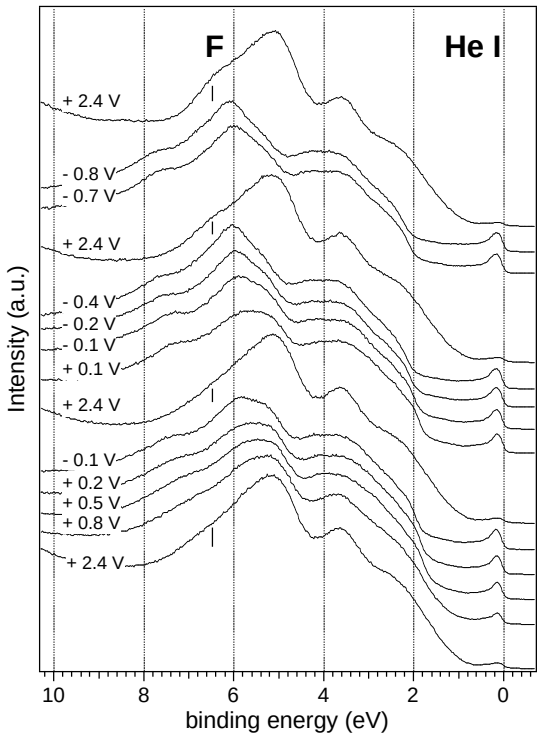

Fig. 5.51 The development of peak F in He I valence spectra upon intercalation-deintercalation cycling

Spectra could be taken following an intercalation-deintercalation cycle at a constant current, which corresponds to a constant intercalation rate (Fig. 5.52). The spectral series shows that with small increments all above discussed effects can be followed: the filling of the Ti 3d states, the opening of the Ti 3d/S 3p gap with shift of the S 3p levels to higher BEs, and the decrease of the work function. Additionally, also the splitting of band E is quite evident. The symmetry of the sharpest peak at 5 eV in the deintercalated film changes possibly in relation to the different stacking of the slabs, which may affect the coupling to the relevant states across the van der Waals gap. The broadening of peak E seems to proceed in parallel with the Ti 2p peak. The intensity of the Ti 3d band saturates for the highly intercalated sample. As Fig. 5.50 shows, this effect is also observed in

He II measurements, but is less evident in valence band spectra measured with X-ray excitation. For instance the Ti 3d intensity is similar for x=0.6 and 0.9 in the He II spectra, but clearly grows in XPS valence band spectra. This may indicate that also with electrochemical intercalation the parallel increased Na coverage may be masking the substrate signals in particular at the Fermi level measured with the low energetic radiation.

All changes of spectral features progress quite smoothly, with no evident transitions, as it should be expected based on the phase changes described by Rouxel *et al.* [34, 225]. Also the voltage-charge curve (insert in Fig. 5.52) does not show any step as it is to expect for phase transitions and has indeed been reported for the Na cells where thick polycrystalline TiS_2 electrodes were used [268-270]. The relevance of grain boundary effects with crystallites at the nanometer scale, the probable presence of large amounts of self-intercalated sites (which means pinned slabs) and structural disorder in general may account for the featureless evolution of all characteristic parameters. It has been reported that in the octahedral coordination the Na diffusivity is lower and it has not been possible to obtain x>0.8 in Na_xTiS_2 at RT either chemically [271] or electrochemically [270]. Due to the nano-sized crystallites, the kinetics of intercalation should not play a decisive role in the present experiment, instead. The progressive core level shift without saturation indeed proves that intercalation occurs for all x values.

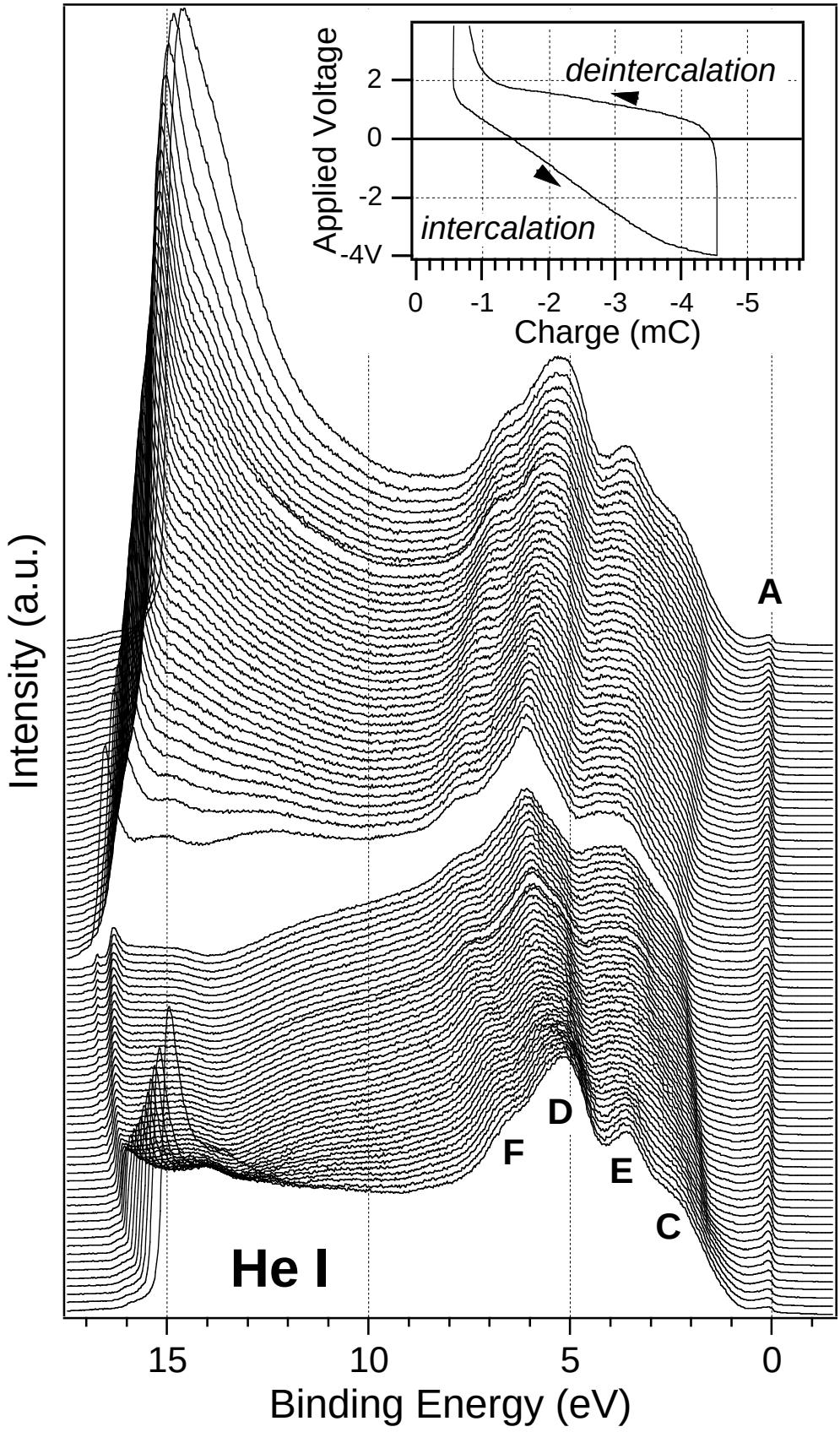

Fig. 5.52 He I valence band spectra recorded during a charge and discharge cycle at a constant current of 1 µA (see inset). Note that a Na concentration x=1 corresponds to a charge of –5 mC

It can be clearly seen that the secondary emission depends dramatically on the cell polarization. The reason for this effect seems to be related to the creation of a Na accumulation or depletion region in the electrolyte next to the cathode interface to the solid electrolyte. In fact, the largest variations are found soon after a current inversion. Indeed the formation of such regions, due to the limited Na^+ mobility in the β''-alumina at RT, is responsible of the voltage drop in non-equilibrium experiments. As a consequence an electric field is built-up which prevents or accelerates the electrons contributing to the secondary onset from the thin TiS_2 surface. This effect, which can be expected at both electrodes, is typical in a cell that is galvanostatically discharged, and is evidenced as a polarization overvoltage. Thus, the secondary emission intensity is sensitive to the formation of this region specifically at the cathode. As in a semiconductor the field associated to this space charge region separates electrons from holes, and the secondary emission strongly depends whether electrons are accelerated towards the TiS_2 cathode. Indeed, it was possible to observe an evident photocurrent when the sample was irradiated with x-rays (Fig. 5.53). This X-ray induced current as measured with the potentiostat is attributed to the separation of electrons in the field produced by Na^+ polarization gradients. With He I irradiation the photocurrent was much smaller, but the presence of secondary electrons is more sensible at low kinetic energy. The sign of the photocurrent was generally, but not strictly, the same as for the dark currents. Although the photocurrent does not corresponds to the Na^+ transfer, its contribution to the calculated electric charges was estimated to be negligible.

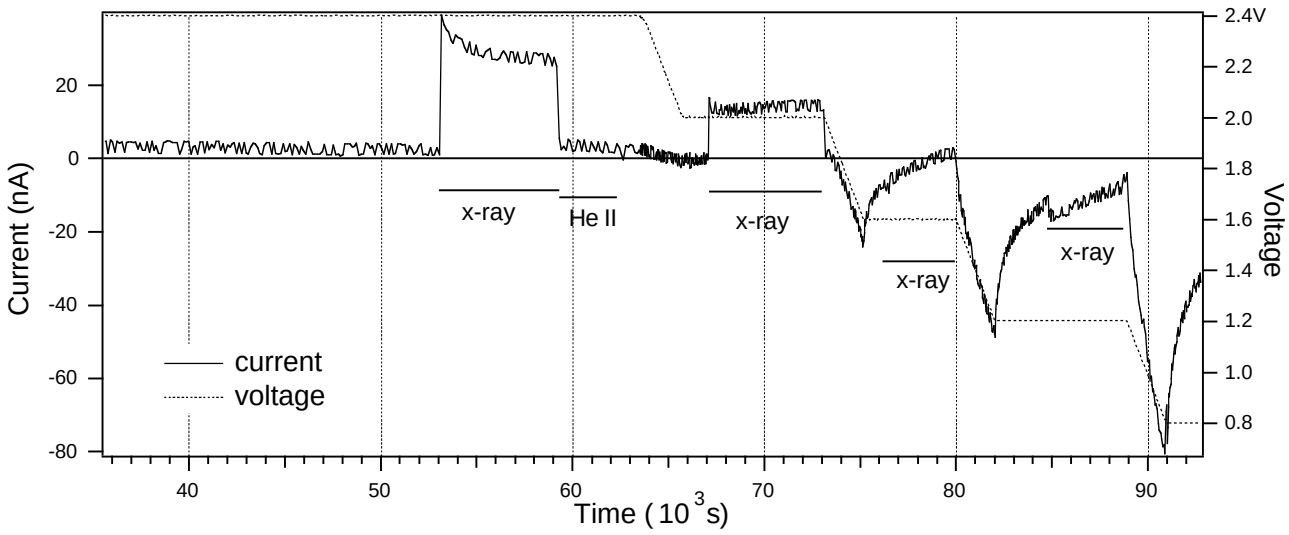

Fig. 5.53 Dependence of the cell current measured at constant voltage on the x-ray excitation

As with Na deposition on a thin film also in this case the main component of the S 2p signal shifts to higher BE, and a new component at higher BE becomes visible. As all other major spectral changes, the new component is completely reversible. This excludes that it corresponds to an irreversible Na decomposition reaction. Na sulfides have a very low free energy of formation and it

is unlikely that they can be reversibly formed. In addition Na_2S should be more ionic than TiS_2, and in the S 2p signal a component at lower binding energy should be expected instead. The new component may be assigned to S of TiS_2 interacting directly with intercalated Na^+. The new S 2p component appears at higher BE and grows as long as the Ti 3d peak in the valence band increases. This may indicate an effect related to the electronic structure more than to the local atomic structure. A charge transfer to S cannot be identified in any new component of the S 2p signal, as it should be expected at low BE. The only possible evidence of charge transfer is the BE shift which is much smaller compared to that observed for other substrate lines.

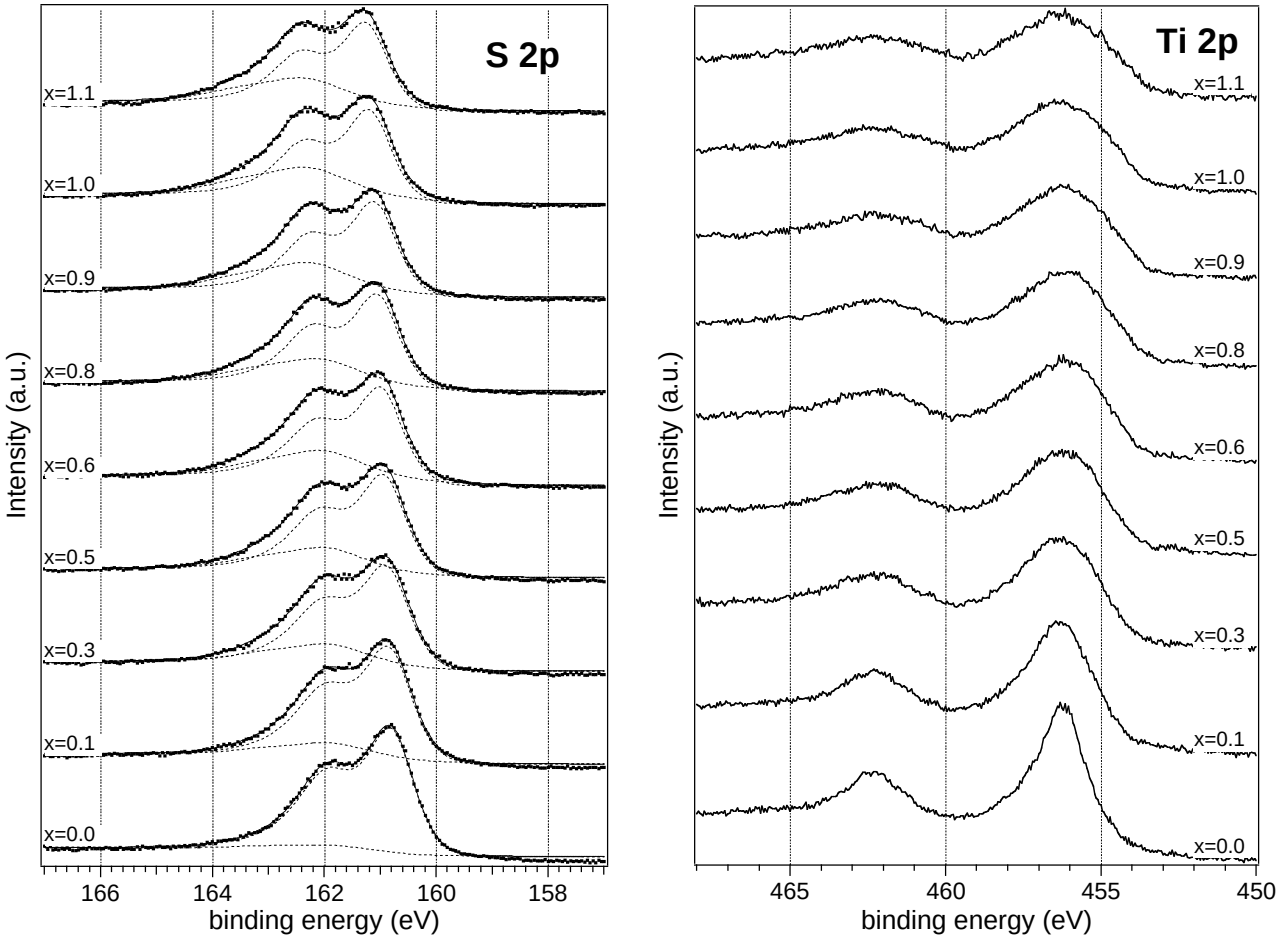

Fig. 5.54 S 2p and Ti 2p core levels for a TiS_2 thin film electrochemically intercalated. Spectra are given with increased Na concentration

The Ti 2p doublet broadens significantly even with small *x*. By increasing *x* the broadening continues, but the appearance of a shoulder seems to be more evident for the highest concentrations (0.8-1.0) and is consistent with the new component observed also by deposition on thin films (Fig. 5.38). Nevertheless the reversibility of this component with reversed voltage scan further supports a phenomenon in relation to the new component for S 2p and excludes the effect of the formation of a stable Na decomposition compound. As in He I valence bands, the effects of the polytype change known with Na intercalation may possibly influence also the Ti 2p peak shape and seems to be the

most reasonable explanation for the observed effect. Probably a large number of components should be used for a fit in dependence of the Na concentration. But with the given energy resolution spectra cannot be fitted within acceptable uncertainty.